

## What is the best RNN-cell structure to forecast each time series behavior?

Rohaifa Khaldi<sup>a</sup> (rohaifa@ugr.es), Abdellatif El Afia<sup>b</sup> (abdellatif.elafia@ensias.um5.ac.ma), Raddouane Chiheb<sup>b</sup> (raddouane.chiheb@ensias.um5.ac.ma), Siham Tabik<sup>a</sup> (siham@ugr.es)

<sup>a</sup> Dept. of Computer Science and Artificial Intelligence, Andalusian Research Institute in Data Science and Computational Intelligence, DaSCI, University of Granada, 18071, Granada, Spain

<sup>b</sup> ENSIAS, Mohammed V University of Rabat, 10170, Rabat, Morocco

### **Corresponding Author:**

Rohaifa Khaldi

Dept. of Computer Science and Artificial Intelligence, Andalusian Research Institute in Data Science and Computational Intelligence, DaSCI, University of Granada, 18071, Granada, Spain

Email: rohaifa@ugr.es

# What is the best RNN-cell structure to forecast each time series behavior?

Rohaifa Khaldi<sup>a,\*</sup>, Abdellatif El Afia<sup>b</sup>, Raddouane Chiheb<sup>b</sup>, Siham Tabik<sup>a</sup>

<sup>a</sup>*Dept. of Computer Science and Artificial Intelligence, Andalusian Research Institute in Data Science and Computational Intelligence, DaSCI, University of Granada, 18071, Granada, Spain*

<sup>b</sup>*ENSIAS, Mohammed V University of Rabat, 10170, Rabat, Morocco*

---

## Abstract

It is unquestionable that time series forecasting is of paramount importance in many fields. The most used machine learning models to address time series forecasting tasks are Recurrent Neural Networks (RNNs). Typically, those models are built using one of the three most popular cells, ELMAN, Long–Short Term Memory (LSTM), or Gated Recurrent Unit (GRU) cells, each cell has a different structure and implies a different computational cost. However, it is not clear why and when to use each RNN-cell structure. Actually, there is no comprehensive characterization of all the possible time series behaviors and no guidance on what RNN cell structure is the most suitable for each behavior. The objective of this study is two-fold: it presents a comprehensive taxonomy of almost all-time series behaviors (deterministic, random-walk, nonlinear, longmemory, and chaotic), and provides insights into the best RNN cell structure for each time series behavior. We conducted two experiments: (1) The first experiment evaluates and analyzes the role of each component in the LSTM-Vanilla cell by creating 11 variants based on one alteration in its basic architecture (removing, adding, or substituting one cell component). (2) The second experiment evaluates and analyzes the performance of 20 possible RNN-cell structures. To evaluate, compare, and select the best model, different statistical metrics were used: error-based metrics, information criterion-based metrics, naïve-based metric, and direction change-based metric. To further improve our confidence in the models' interpretation and selection, Friedman Wilcoxon–Holm signed-rank test was used.

Our results advocate the usage and the exploration of the newly created RNN variant, named SLIM, in time series forecasting thanks to its high ability to accurately predict the different time series behaviors as well as its simple structural design that does not require expensive temporal and computing resources.

**Keywords:** Forecasting, Time series, Times series behavior, RNN models, LSTM cells, Performance evaluation metrics

---

## 1. Introduction

Many real-world prediction problems involve a temporal dimension and typically require the estimation of numerical sequential data referred to as time series forecasting. Time series forecasting is one of the major

---

\*Corresponding author.

Email addresses: [rohaifa@ugr.es](mailto:rohaifa@ugr.es) (Rohaifa Khaldi ), [abdellatif.elafia@ensias.um5.ac.ma](mailto:abdellatif.elafia@ensias.um5.ac.ma) (Abdellatif El Afia), [raddouane.chiheb@ensias.um5.ac.ma](mailto:raddouane.chiheb@ensias.um5.ac.ma) (Raddouane Chiheb), [siham@ugr.es](mailto:siham@ugr.es) (Siham Tabik)

stones in data science playing a pivotal role in almost all domains, including meteorology (Murat et al. 2018), natural disasters control (Erdelj et al. 2017), energy (Bourdeau et al. 2019), manufacturing (Wang & Chen 2018), finance (Liu 2019), econometrics (Siami-Namini & Namin 2018), telecommunication (Maeng et al. 2020), healthcare (Khaldi et al. 2019b) to name a few. Accurate time series forecasting requires robust forecasting models.

Currently, Recurrent Neural Network (RNN) models are one of the most popular machine learning models in sequential data modeling, including natural language, image/video captioning, and forecasting (Sutskever et al. 2014, Vinyals et al. 2015, Chimmula & Zhang 2020). Such RNN models are built as a sequence of the same cell structure, for example, ELMAN cell, Long-Short Term Memory (LSTM) cell or Gated Recurrent Unit (GRU) cell. The simplest RNN cell is ELMAN, it includes one layer of hidden neurons. While, LSTM and GRU cells incorporate a gating mechanism, three gates in LSTM and two gates in GRU, where each gate is a layer of hidden neurons. Many other cell structures have been introduced in the literature (Zhou et al. 2016, Lu & Salem 2017, Mikolov et al. 2014, Pulver & Lyu 2017). However, to solve time series forecasting tasks, the building of RNN models is typically limited to the three aforementioned cell structures (Sezer et al. 2020, Runge & Zmeureanu 2021, Liu et al. 2021, Rajagukguk et al. 2020, Alkhayat & Mehmood 2021), as they provide very good accuracy (Runge & Zmeureanu 2021, Sezer et al. 2020).

Nevertheless, building robust RNN models for time series forecasting is still a challenging task as there does not exist yet a clear understanding of times series data itself and hence there exist very little knowledge about what cell structure is the most appropriate for each data type. In general, when facing a new problem, practitioners select one of the most popular cells, usually LSTM, and use it as a building block for the RNN model without any guarantee on the appropriateness of this cell to the current data. The objective of this work is two-fold. It presents a comprehensive characterization of time series behaviors and provides guidelines on the best RNN cell structure for each behavior. As far as we know, this is the first work providing such insights. The main contributions of this study can be summarized as follows:

- Provide a better understanding of times series data by presenting a comprehensive characterization of their behaviors.
- Determine the most appropriate cell structure for each time series behavior (i.e., whether a specific cell structure should be avoided for certain behaviors).
- Identify differences in predictability between behaviors (i.e., whether certain behaviors are easier or harder to predict across all cell models).
- Provide useful guidelines that can assist decision-makers and scholars in the process of selecting the most suitable RNN-cell structure from both, a computational and performance point of view.

The remainder of this study is organized as follows: Section 2 states the related works. Section 3 presents a taxonomy of time series behaviors. Section 4 presents a taxonomy of RNN cells. Section 5 describes the

experiment. Section 6 exhibits and discusses the obtained results. Finally, the last section concludes the findings and spots light on future research directions.

## 2. Related works

The last decades have known an explosion of time series data acquired by automated data collection devices such as monitors, IoT devices, and sensors (Murat et al. 2018, Erdelj et al. 2017, Bourdeau et al. 2019). The collected time series describes different quantitative values: stock price, amount of sales, electricity load demand, weather temperature, etc. In parallel, a large number of comparative studies have been carried out in the forecasting area (Parmezan et al. 2019, Godahewa et al. 2021, Athiyarath et al. 2020, Divina et al. 2019, Choubin et al. 2018, Sagheer & Kotb 2019, Bianchi et al. 2017). These studies can be divided into two categories: (1) the first category tries to find a universal forecasting model for any field (Parmezan et al. 2019, Godahewa et al. 2021, Athiyarath et al. 2020). They compare multiple models on a set of datasets from different fields to conclude which model is the universal predictor. The selection of the used datasets is not based on any clear criteria. Whereas, (2) the second category focuses on selecting the most performing forecasting model for a specific field (Divina et al. 2019, Choubin et al. 2018, Sagheer & Kotb 2019, Bianchi et al. 2017). They compare a set of models on one or multiple datasets coming from the same field. Nevertheless, the best predictor does not ensure stable performance over different datasets even if they come from the same field. Actually, after an extensive analysis of highly diverse datasets, (Keogh & Kasetty 2003) demonstrated that there is a need for more comprehensive time series benchmarks and more careful evaluations in the data mining community. In addition, datasets should have a large size to train and test the models and incorporate specific behaviors that challenge their modeling. Such knowledge of the dataset properties is required to facilitate a better interpretation of the modeling results.

The natural approach to create such benchmarking time series datasets is to collect data from real applications. For instance, the NN5 dataset (Crone 2008), the CIF 2016 dataset (Godahewa et al. 2020), the M4 dataset (Makridakis et al. 2018), and the Monash archive that gather 20 publicly available time series datasets (Godahewa et al. 2021). Although, real time series are always business-oriented which make them either proprietorial or expensive to obtain (Dau et al. 2019), they can take decades to become mature and ready to be used for machine learning purposes, their diversity testing is tedious (Dau et al. 2019, Spiliotis et al. 2020), and most importantly, their Data Generation Processes (DGPs) are unknown which make the interpretation of the models and the explanation of their decisions challenging.

An alternative solution is to generate synthetic time series datasets with known embedded patterns (Olson et al. 2017). For instance, (Zhang & Qi 2005) investigated the issue of how to effectively model artificial time series with deterministic behavior due to the existence of trend and seasonality using Artificial Neural Networks (ANNs). (López-Caraballo et al. 2016) examined ANNs on time series with noiseless and noisy chaotic behavior generated by Mackey-Glass series. (Li & Lin 2016) applied the Self-Constructing Fuzzy Neural Network (SCFNN) on chaotic time series including Logistic and Henon data. (Yeo 2017)

evaluated the performance of LSTM on three different time series with chaotic behavior (delay-time chaotic dynamical systems, Mackey-Glass and Ikeda equations). (Fischer et al. 2018) presented an experimental evaluation of seven machine learning models applied on a set of eight DGPs reflecting linear and nonlinear behaviors. (Parmezan et al. 2019) used 40 synthetic datasets of deterministic, stochastic, and chaotic time series to compare eleven parametric and non-parametric models. (Kang et al. 2020) used the Mixture Auto-Regressive (MAR) models to create the GRATIS dataset based on which they compared different statistical models. However, all the aforementioned studies remain non-comprehensive of the main time series behaviors that can be faced in real datasets.

Another categorization of these comparative studies can be made based on the types of the evaluated models. Here, three categories can be set: (1) Studies based on parametric models where scientists try to evaluate the forecasting performance of different statistical models (Godahewa et al. 2021, Yu et al. 2020, Kim & Jung 2018). (2) Studies based on non-parametric models where they assess the performance of machine learning models (Granata 2019, Dudek 2016, Sagheer & Kotb 2019). (3) Studies based on parametric and non-parametric models where both types of models are compared (Parmezan et al. 2019, Khaldi et al. 2019a, Yamak et al. 2019, Siami-Namini & Namin 2018). RNNs are one of the most used machine learning models in time series forecasting (Sezer et al. 2020). Nevertheless, their usage is limited to three RNN variants (ELMAN, LSTM, and GRU). In the financial field, (Sezer et al. 2020) reported that from 2005 to 2019, 52.5% of publications used RNN models to perform time series forecasting, where the LSTM model represents 60.4%, ELMAN (vanilla RNN) represents 29.7%, and GRU represents 9.89%. In the energy field, (Runge & Zmeureanu 2021) stated in their review that ELMAN, GRU, and LSTM are the main applied deep learning models to building energy forecasting. In the environmental field, (Liu et al. 2021) asserted in their review, from 2015 to 2020, that LSTM and GRU are the most practical RNN models in air quality forecasting. In the renewable energy field, (Rajagukguk et al. 2020) reviewed, from 2005 to 2020, that in photovoltaic power forecasting, 60% of publications used LSTM, 20% used ELMAN, and 13% used GRU. While, in the solar irradiance forecasting, they reported that LSTM represents 44% of the used deep learning models, ELMAN represents 25% and GRU 19%. Similarly, (Alkhayat & Mehmood 2021) reported in their review, from 2016 to 2020, that ELMAN, LSTM, and GRU are the only RNN models used in wind and solar energy forecasting. They outlined that the usage of RNNs within this field increased from 2% in 2016 to 25% in 2020.

Therefore, there is a strong need for a comprehensive analysis of different types of RNN models, including the above three variants, in forecasting the main time series behaviors, and a strong need for an RNN-based model guide to assist practitioners in their process of selection and structure of the best RNN cell for each time series behavior.

### 3. Taxonomy of times series behaviors

As far as we know, this is the first work introducing a complete formal characterization of real-world time series. Time series emerging from real-world applications can either follow a stochastic mechanism or a chaotic mechanism and are usually contaminated by white noise (Wales 1991, Cencini et al. 2000, Zunino et al. 2012, Box et al. 2015, Boaretto et al. 2021).

#### 3.1. Stochastic behavior

In stochastic behavior, real times series are generated by a random stable system, and can exhibit the following behaviors:

1. Deterministic behavior. These time series are characterized by the existence of deterministic patterns. They usually incorporate at least one of the following patterns: increasing or decreasing deterministic trend, simple deterministic seasonality, and complex deterministic seasonality (Figure 1). The trend pattern is a long-term evolution in the data, it can be increasing or decreasing, and it can have different forms (linear, exponential, and damped) (Montgomery et al. 2015). An increasing trend can appear in the demand for technologies in the social fields, while a decreasing trend is related to epidemics, mortality rates, and unemployment (Parmezan et al. 2019). The seasonality pattern can be described as the occurrence of short-term regular variation that repeats at known and relatively constant time intervals. This type of pattern can occur in different types of data including time series of sales, e.g., the increase in sales of warm clothing in winter and air conditioners in summer (Parmezan et al. 2019).
2. Random-Walk behavior. The time series of this behavior are characterized by the existence of unit-root patterns. This behavior appears when the time series have a stochastic increasing or decreasing trend and/or stochastic seasonality (Figure 2). Here the current observation is equal to the previous observation plus a random step. The lag between these two observations is equal to one in the case of trend and equal to the seasonality period in the case of seasonality.

The presence of deterministic or random-walk behavior induces the non-stationarity in time series. The stationarity is a relevant feature in time series which basically implies that the mean, the variance, and the covariance do not depend on time (Montgomery et al. 2015). These two types of behaviors are the most important features in time series, and usually characterize business and macro-economic data (Salles et al. 2019, Liu et al. 2019).

3. Nonlinear behavior. Time series observations can often exhibit correlations with different degrees of non-linearity (Figure 3). This type of behavior is present in almost all real-world time series data, such as in stream-flow forecasting (Wang et al. 2020), and in financial markets forecasting (Bukhari et al. 2020).

4. Long-memory behavior. Some time series may present properties of long-range dependencies in time which implies a strong coupling effect between the values of observations at different time steps, i.e. the correlations between observations has a slower exponential decay compared to short-range dependencies (Figure 4). This type of behavior can occur in hydrology forecasting (Papacharalampous & Tyralis 2020), network traffic forecasting (Ramakrishnan & Soni 2018), financial market forecasting (Bukhari et al. 2020), etc.

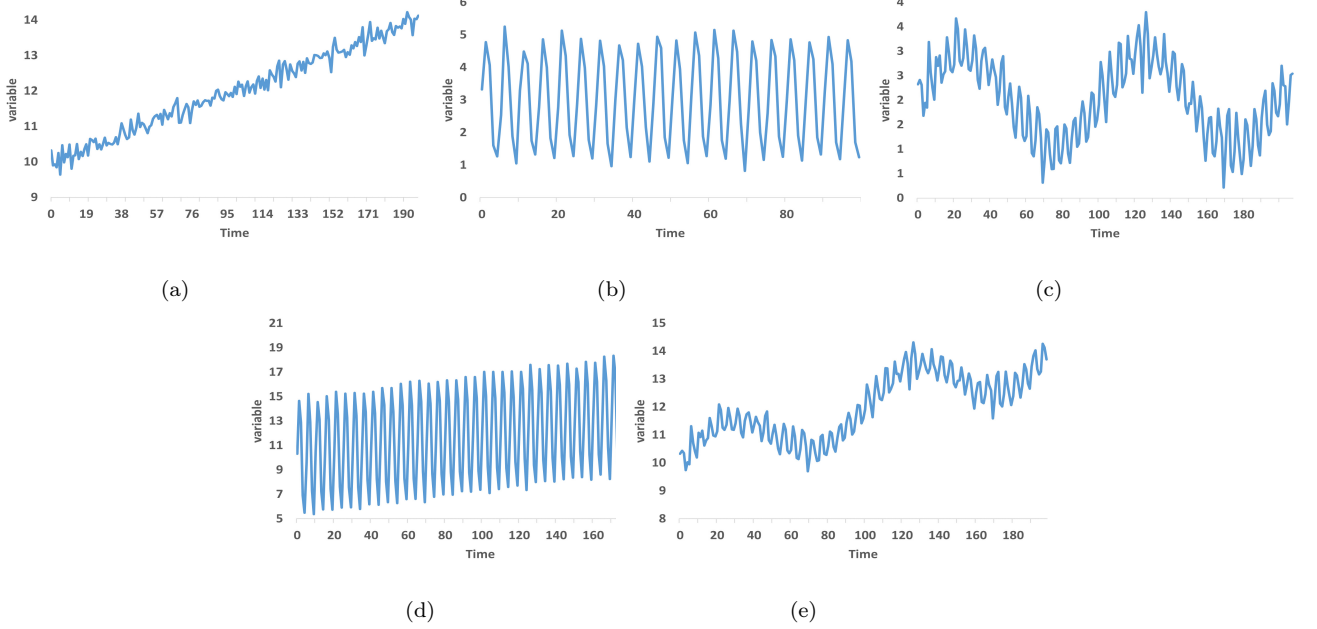


Figure 1: Time series with deterministic behavior: (a) increasing trend, (b) simple seasonality, (c) complex seasonality, (d) increasing trend and simple seasonality and (e) increasing trend and complex seasonality.

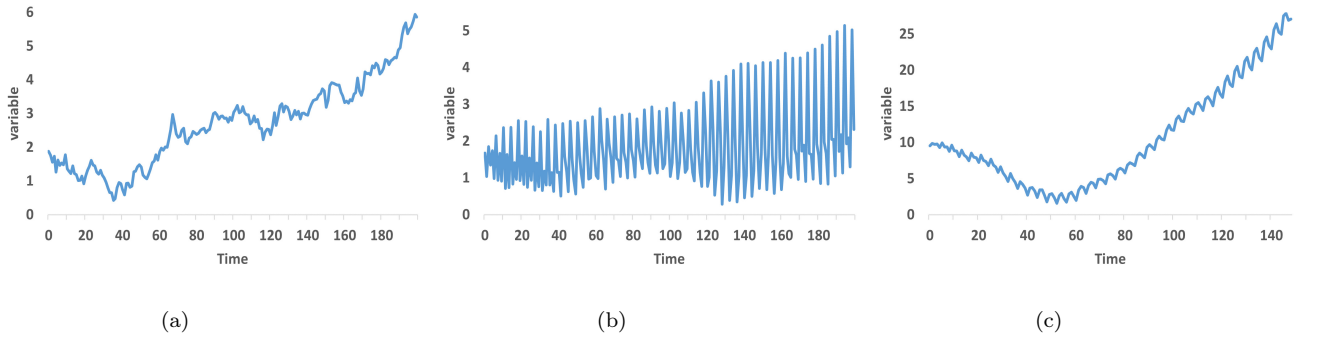


Figure 2: Time series with random-walk behavior: (a) trend random-walk, (b) seasonal random-walk, (c) trend and seasonal random-walk.

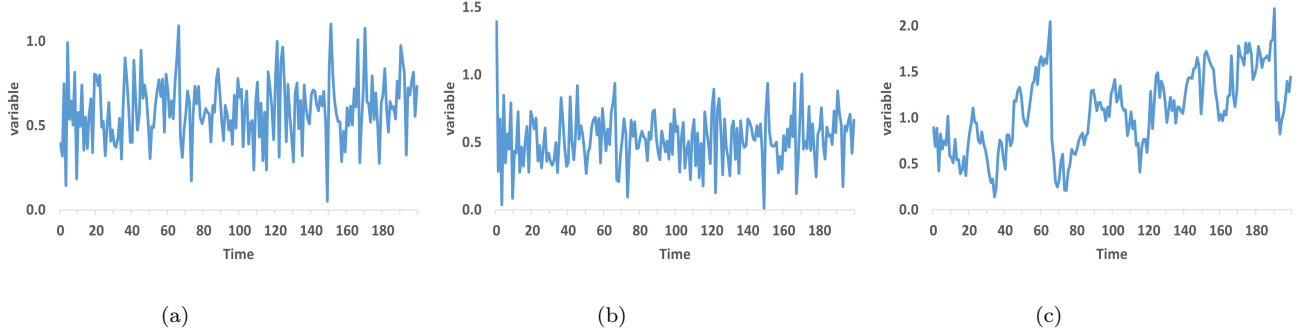


Figure 3: Time series with nonlinear behavior generated by: (a) Nonlinear Auto-Regressive (NAR) process, (b) Smooth Transition Auto-Regressive (STAR) process, (c) Threshold Auto-Regressive (TAR) process.

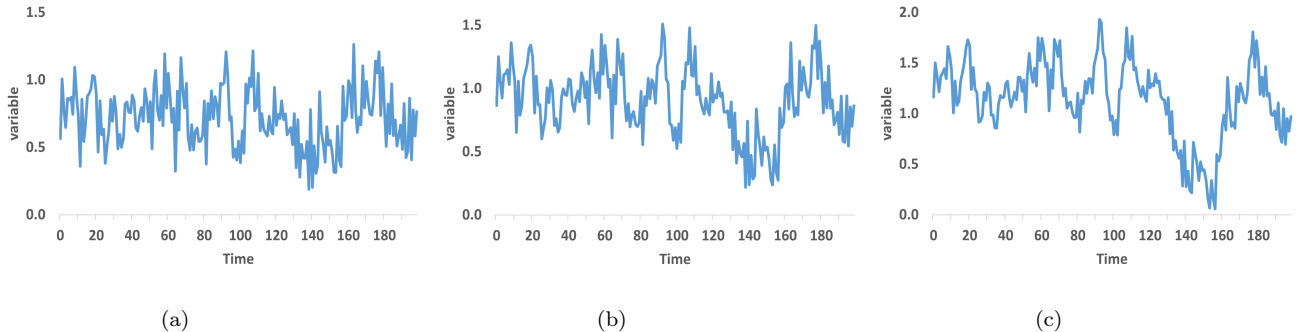


Figure 4: Time series with long-memory behavior: (a) short memory generated by ARFIMA(2,0.0,2), (b) long memory generated by ARFIMA(2,0.2,2) and (c) long memory generated by ARFIMA(2,0.4,2).

### 3.2. Chaotic behavior

The chaotic mechanism can be expressed as a nonlinear deterministic dynamical system that is often unknown or incompletely understood (Li & Lin 2016). Real-time series can exhibit a noisy chaotic behavior (Figure 5), these time series are sensitive to initial conditions (butterfly effect) where small smooth perturbations in the system or measurement errors generate an abrupt change in the behavior of the time series (bifurcation). This type of behavior is unstable since it tends to be deterministic in short term but random in long term. Such kind of time series are usually present in many sciences and engineering fields such as weather forecasting (Tian 2019), financial markets forecasting (Bukhari et al. 2020), energy forecasting (Bourdeau et al. 2019), intelligent transport and trajectory forecasting (Giuliani et al. 2021), etc.

Based on the literature (Chandra & Zhang 2012, Montgomery et al. 2015, Liu et al. 2017, Fischer et al. 2018), the five aforementioned behaviors (deterministic, random-walk, nonlinear, long-memory, and chaotic) are the main behaviors encountered in real applications. Real-world time series can either express an individual behavior or an aggregation of more than one behavior. To identify which type of behavior a real-world time series can include, different statistical preprocessing tools and tests can be applied (Grau-Carles 2005, Inglada-Perez 2020). In Table 1, we present a set of tools that can be used to identify the existence of the five aforementioned behaviors in time series data.

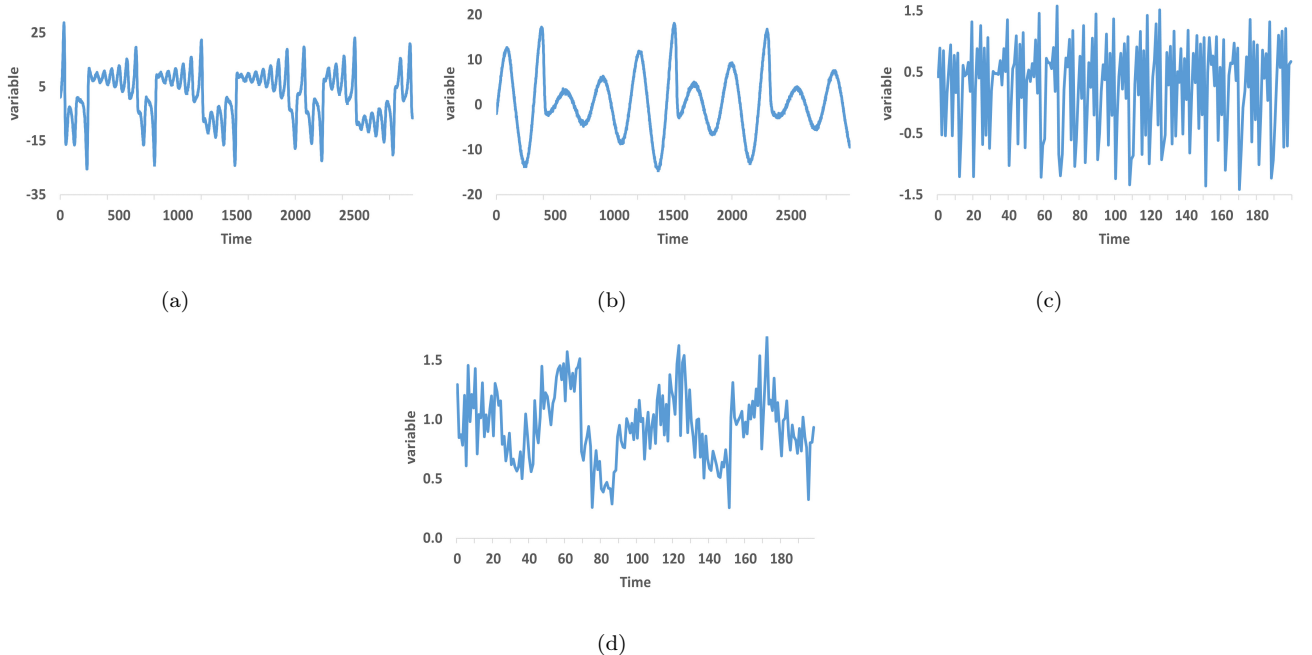


Figure 5: Time series with noisy chaotic behavior: (a) TS generated by Lorenz process. (b) TS generated by Rössler process. (c) TS generated by Hénon map process. (d) TS generated by Mackey-Glass process.

#### 4. Taxonomy of RNN cells

Humans do not start their thinking from zero every second, our thoughts have persistence in the memory of our brains. For example, as the reader reads this paper, he/she understands each word based on his/her understanding of the words before. The absence of memory is the major shortcoming in traditional machine learning models, particularly in feed-forward neural networks (FNNs). To overcome this limitation, RNNs integrate the concept of feedback connections in their structure (Figure 6, where  $x_t$  and  $h_t$  are the input state and the hidden state at time step  $t$ , respectively). This mechanism enables RNNs to have a certain memory capable of capturing the dynamics in sequential data by conveying information through time.

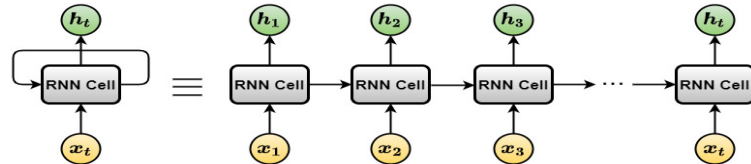


Figure 6: The folded (left) and unfolded (right) architecture of RNN model.

Table 1: A set of tools used to identify the five different time series behaviors.

Tool	Time series behavior	Reference
Data visualization	Deterministic behavior	(Chatfield 2013)
Correlogram	Deterministic behavior	(Box et al. 2015)
Time series decomposition	Deterministic behavior	(Chatfield 2013)
Smoothing	Deterministic behavior	(Montgomery et al. 2015)
Data visualization	Random-Walk behavior	(Montgomery et al. 2015)
Augmented Dickey Fuller (ADF) test	Random-Walk behavior	(Dickey & Fuller 1979)
Phillips–Perron (PP) test	Random-Walk behavior	(Phillips & Perron 1988)
Kwiatkowski–Phillips–Schmidt–Shin (KPSS) test	Random-Walk behavior	(Kwiatkowski et al. 1992)
Kaplan test	Nonlinear behavior	(Kaplan 1994)
Keenan test	Nonlinear behavior	(Keenan 1985)
Tsay test	Nonlinear behavior	(Tsay 1986)
Teräsvirta test	Nonlinear behavior	(Teräsvirta et al. 1993)
White test	Nonlinear behavior	(White 1989)
Correlogram	Long-memory behavior	(Palma 2007)
Qu test	Long-memory behavior	(Qu 2011)
R/S analysis	Long-memory behavior	(Mandelbrot & Wallis 1968)
Modified R/S	Long-memory behavior	(Lo 1991)
Geweke and Porter-Hudak (GPH) test	Long-memory behavior	(Geweke & Porter-Hudak 1983)
Detrended Fluctuation Analysis (DFA)	Long-memory behavior	(Peng et al. 1994)
Correlation Dimension	Chaotic behavior	(Grassberger & Procaccia 1984)
Lyapunov Exponent	Chaotic behavior	(Bensaïda & Litimi 2013)
MGRM test	Chaotic behavior	(Matilla-García & Marín 2010)
Recurrence Plots	Chaotic behavior	(Eckmann & Ruelle 1985)
0/1 test	Chaotic behavior	(Gottwald & Melbourne 2004)

Table 2: A collection of RNN cell structures historically sorted.

RNN cell structure	Year	Reference
JORDAN	1989	(Jordan 1989)
ELMAN	1990	(Elman 1990)
LSTM-NFG	1997	(Hochreiter & Schmidhuber 1997)
LSTM-Vanilla	2000	(Gers et al. 2000)
LSTM-PC	2000	(Gers & Schmidhuber 2000)
SCRN	2014	(Mikolov et al. 2014)
GRU	2014	(Cho et al. 2014)
IRNN	2015	(Le et al. 2015)
LSTM-FB1	2015	(Jozefowicz et al. 2015)
MUT	2015	(Jozefowicz et al. 2015)
LSTM-CIFG	2015	(Nina & Rodriguez 2015)
Differential LSTM	2015	(Veeriah et al. 2015)
MRNN	2016	(Abdulkarim 2016)
MGU	2016	(Zhou et al. 2016)
Phased LSTM	2016	(Neil et al. 2016)
Highway Connections	2016	(Irie et al. 2016)
LSTM with Working Memory	2017	(Pulver & Lyu 2017)
SLIM	2017	(Lu & Salem 2017, Dey & Salem 2017, Heck & Salem 2017)
GORO	2019	(Jing et al. 2019)

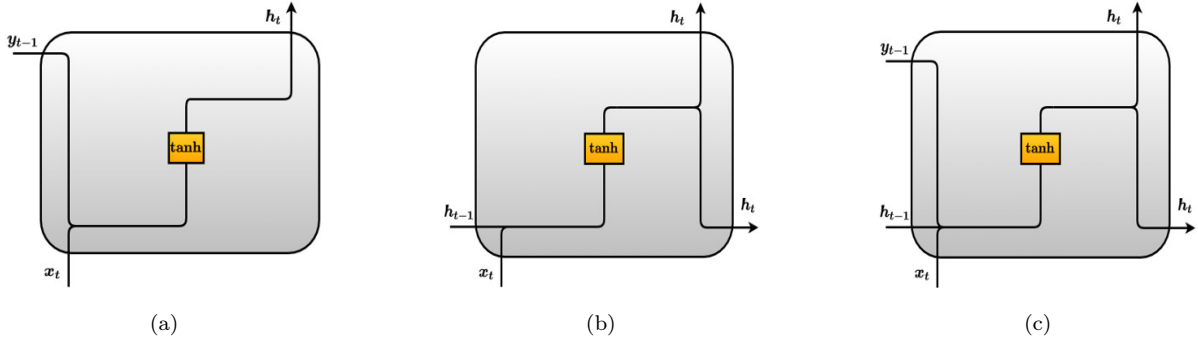


Figure 7: (a) JORDAN cell structure. (b) ELMAN cell structure. (c) MRNN cell structure.

RNN models are built based on one specific cell structure which is the core of all computations that occur in the network. Multiple cell structures have been created since 1989 (Table 2). The early cell structure is named JORDAN (Jordan 1989), where at each time step the previous output state is fed into the cell (Figure 7a). Later, the ELMAN cell was proposed by (Elman 1990). Unlike the JORDAN cell, each time step in the ELMAN cell calls the previous hidden state (Figure 7b). In 2016, a combination of both JORDAN and

ELMAN cells in one cell named multi-recurrent neural network (MRNN) was evaluated by (Abdulkarim 2016). In this cell structure, at each time step, both previous output and hidden states are presented to the cell (Figure 7c).

It was proved that the ELMAN cell suffers from the vanishing and exploding gradient problems that impede the capturing of long-term dependencies (Pascanu et al. 2013). To overcome the memory limitation of this cell, novel cell structures have been proposed. In 2014, the Structurally Constrained Recurrent Network (SCRN) was proposed by (Mikolov et al. 2014). They integrated a slight structural modification in the ELMAN cell that consists in adding a new slowly changing state at each time step called context state  $s_{t-1}$  (Figure 8a). In 2015, (Le et al. 2015) created a new cell called Identity Recurrent Neural Network (IRNN) as a modification of ELMAN by setting the ReLu as the activation function, the identity matrix as an initialization of the hidden states weight matrix, and zero as an initialization of the bias (Figure 8b).

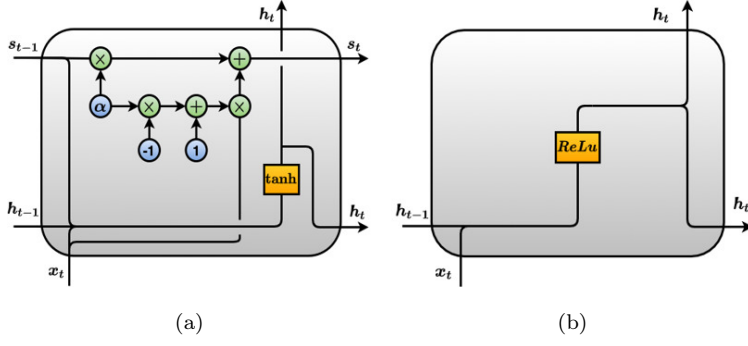


Figure 8: (a) SCRN cell structure. (b) IRNN cell structure.

A different way to handle the vanishing and exploding gradient problems resulted in creating different cell structures characterized by the gating mechanism that regulates the flowing of the information flux. The gates can be seen as filters that only hold useful information and selectively remove any irrelevant information from passing through. To perform this control of information (i.e., which information to pass and which information to discard), the gates are equipped with parameters that need to be trained through the model learning process using the back-propagation through time algorithm (Werbos 1990). Thus, this mechanism provides the RNN cell with an internal permanent memory able to store information for long time periods (Weston et al. 2014, Graves et al. 2014).

In 1997, the first version of this type of cell named Long-Short Term Memory with No Forget Gate (LSTM-NFG) was created by (Hochreiter & Schmidhuber 1997). This cell contains two gates: the input gate  $\Gamma_{i_t}$  and the output gate  $\Gamma_{o_t}$ . Later in 2000, the concept of the forget gate  $\Gamma_{f_t}$  was introduced by (Gers et al. 2000) creating LSTM-Vanilla that has been widely used in most applications (Figure 9a). In the same year, the LSTM cell with peephole connections (LSTM-PC) was proposed by (Gers & Schmidhuber 2000). The peephole connections connect the previous cell state  $c_{t-1}$  with the input, forget, and output gates (Figure 9b). These connections enable the LSTM cell to inspect its current cell states (Gers & Schmidhuber 2001), and to learn precise and stable timing without teacher forcing (Gers et al. 2002).

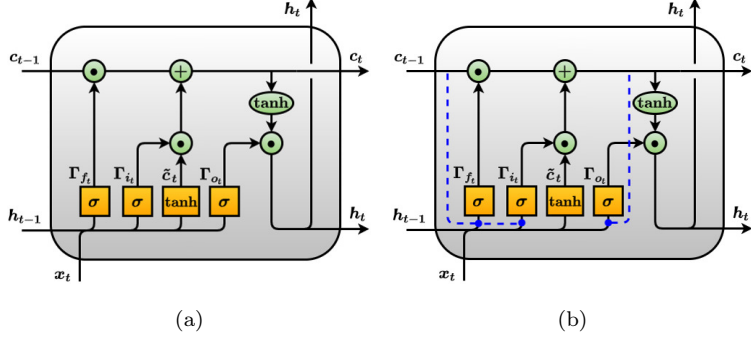


Figure 9: (a) LSTM-Vanilla cell structure. (b) LSTM-PC cell structure.

In 2014, the Gated Recurrent Unit (GRU) cell was proposed by (Cho et al. 2014) as a simpler variant of LSTM that shares many of the same properties. The idea behind GRU cell was to reduce the gating mechanism of LSTM cell from three gates to two gates (relevance gate  $\Gamma_{r_t}$  and update gate  $\Gamma_{u_t}$ ) in order to decrease the number of parameters and to improve the learning velocity (Figure 10a). In 2015, ten thousand RNN cell structures were evaluated by (Jozefowicz et al. 2015) using a mutation-based search process. They identified a new cell architecture that outperforms both LSTM and GRU on some tasks. This cell consists in adding a bias of 1 to LSTM forget gate creating the LSTM-FB1 cell. Further, they discovered three optimal cell architectures named MUT1, MUT2, and MUT3 that are similar to GRU but have some modifications in their gating mechanism and in their candidate hidden state  $\tilde{h}_t$  (Figure 10b and 10c). During that year, coupling both the input and the forget gates into one gate was proposed by (Nina & Rodriguez 2015) creating the LSTM-CIFG cell (Figure 11a). Further, the differential LSTM cell was proposed by (Veeriah et al. 2015) to solve the impact of spatial-temporal dynamics by introducing the differential gating scheme in LSTM cell.

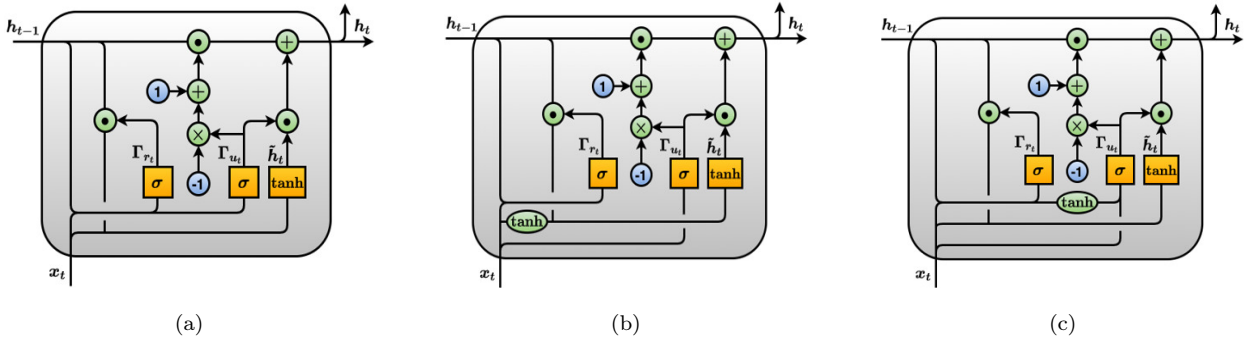


Figure 10: (a) GRU cell structure. (b) MUT1 cell structure. (c) MUT3 cell structure.

In 2016, the Minimal Gate Unit (MGU) cell was created by (Zhou et al. 2016) to further reduce the number of parameters by decreasing the gating mechanism to one forget gate. This variant has a simpler structure and fewer parameters compared to LSTM and GRU cells (Figure 11b). In the same year, eight variants of LSTM-PC cell (based on modifying, adding, or removing one cell component at each time) were evaluated by (Greff et al. 2016) on three different types of tasks: speech recognition, polyphonic music modeling, and handwritten recognition. They demonstrated that the forget and the output gates are the most critical

components in LSTM cell. In addition, their results show that none of the evaluated variants can overcome the LSTM-PC cell. During that year, the phased LSTM cell was introduced by (Neil et al. 2016), where they added a time gate that updates the cell sparsely, and makes it converge faster than the basic LSTM. Further, highway connections were added to GRU and LSTM cells by (Irie et al. 2016). In 2017, LSTM with working memory was created by (Pulver & Lyu 2017), where they substituted the forget gate with a functional layer whose input depends on the previous cell state. In 2019, a Gated Orthogonal Recurrent Unit (GORO) was introduced by (Jing et al. 2019), where they added to the GRU cell an orthogonal matrix that replaced the hidden state loop matrix.

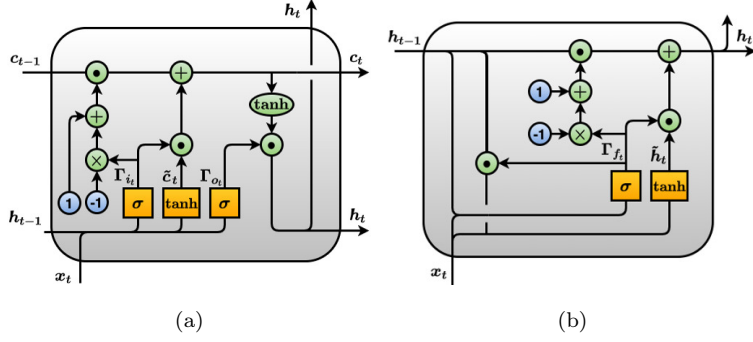


Figure 11: (a) LSTM-CIFG cell structure. (b) MGU cell structure.

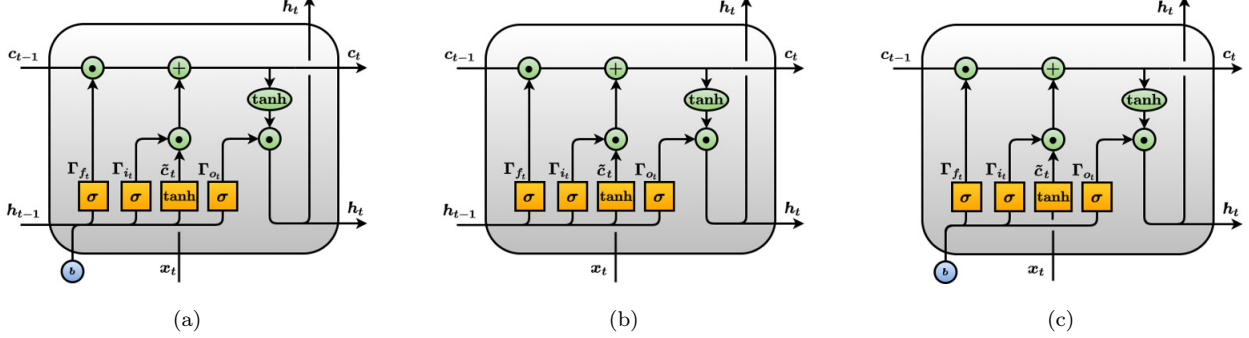


Figure 12: (a) SLIM1 cell structure. (b) SLIM2 cell structure. (c) SLIM3 cell structure.

While very powerful in long-term dependencies, the basic cells (LSTM, GRU, and MGU) have a complex structure with a relatively large number of parameters. In 2017, the concept of parameter reduction was differently tackled through the creation of new cells called SLIM (Lu & Salem 2017, Dey & Salem 2017, Heck & Salem 2017) while maintaining the same number of gates in the basic cells. These variants aim to reduce aggressively the parameters in order to achieve memory and time savings while necessarily retaining a performance comparable to the basic cells. The new parameter-reduced variants of the basic cells eliminate the combinations of the input state, the hidden state, and the bias from the individual gating signals, creating SLIM1, SLIM2, and SLIM3, respectively. The SLIM1 cell consists in removing from the mechanism of all the gates the input state and its associated parameter matrix (Figure 12a). The SLIM2 cell consists in maintaining only the hidden state and its associated parameter matrix (Figure 12b). Whereas, the SLIM3

cell consists in removing the input state, the hidden state, and their associated parameters matrices (Figure 12c). The cellular calculations within the displayed RNN cells along with the evaluated ones are provided in Appendix.

## 5. Experimental structure

Two experiments have been carried out in this study. The first experiment analyzes the utility of each LSTM-Vanilla cell component in forecasting time series behaviors. The second experiment evaluates different variants of RNN cell structures in forecasting time series behaviors. In this section, we first describe the process we followed to generate the dataset for each time series behavior (Section 5.1). Then, we present the selected models for the first and the second experiment (Section 5.2). Finally, we provide the setup of the used models (Sections 5.3, 5.4, 5.5, and 5.6).

### 5.1. Synthetic data generation

To simulate the five aforementioned time series behaviors, we used 21 different DGPs with white Gaussian noise  $\epsilon_t \sim \mathcal{N}(\mu = 0, \sigma = 0.2)$ . From each DGP we created time series of length 3000 observations replicated 30 times through a Monte Carlo simulation experiment using different initial random seeds for the white noise term  $\epsilon_t$  (Table 3).

To generate time series with deterministic behavior, 5 DGPs were used (Table 4): Trend process (T), Simple Seasonality process (SS), Complex Seasonality process (CS), Trend and Simple Seasonality process (TSS), and Trend and Complex Seasonality process (TCS). To simulate the random-walk behavior, 3 DGPs were used (Table 6): Trend Random-Walk process (TRW), Seasonal Random-Walk process (SRW), and Trend and Seasonal Random-Walk process (TSRW). To simulate time series with nonlinear behavior, we used 6 most popular nonlinear models commonly used in the forecasting literature having an increasing level of non-linearity (Zhang et al. 2001) (Table 5): Sign Auto-Regressive process (SAR), Nonlinear Moving Average process (NMA), Nonlinear Auto-Regressive process (NAR), Bilinear process (BL), Smooth Transition Auto-Regressive process (STAR), and Threshold Auto-Regressive process (TAR). These models are motivated by many nonlinear characteristics commonly observed in practice. To artificially generate time series with long memory behavior, we used the Auto-Regressive Fractionally Integrated Moving Average process ARFIMA(p,d,q) since it is one of the best-known long memory processes (Liu et al. 2017). In order to evaluate the performance of RNN cell structures with respect to DGPs with an increasing memory structure, 2 DGPs were created based on the variation of the fractional order of ARFIMA process  $d = \{0.2, 0.4\}$ . A higher fractional order  $d$  implies longer dependency structure (Table 7). To ensure the stationarity of the generated time series, we set the values of the fractional order strictly less than 0.5. Finally, to simulate the noisy chaotic behavior, the 4 most known chaotic DGPs were used (Table 8): Mackey-Glass process, Lorenz process, Rössler process, and Hénon-Map process. Then, we added the white Gaussian noise  $\epsilon_t$  to the deterministic signals to create noisy chaotic time series (Sangiorgio et al. 2021).

Table 3: Number of data generation processes and time series in each behavior, and the number of hyperparameter selection experiments per model in each behavior.

Behavior	# DGPs	# Time series	# Experiments per model
Deterministic behavior	5	150	50
Random-walk behavior	3	90	30
Nonlinear behavior	6	180	60
Long-memory behavior	2	60	20
Chaotic behavior	4	120	40
Total	20	600	200

Table 4: The DGPs used to simulate time series with deterministic behavior.

Process name	Process mathematical model
Trend process	$(T) : z_t = 10 + 0.02t + \epsilon_t$
Simple Seasonality process	$(SS) : z_t = 2 \sin(2\pi t/5) + \epsilon_t$
Complex Seasonality process	$(CS) : z_t = \sin(2\pi t/100) + 0.5 \sin(2\pi t/5) + \epsilon_t$
Trend and Simple Seasonality process	$(TSS) : z_t = 10 + 0.02t + 5 \sin(2\pi t/5) + \epsilon_t$
Trend and Complex Seasonality process	$(TCS) : z_t = 10 + 0.02t + \sin(2\pi t/100) + 0.5 \sin(2\pi t/5) + \epsilon_t$

Table 5: The DGPs used to simulate time series with nonlinear behavior.

Process name	Process mathematical model
	$SAR(2) : z_t = sign(z_{t-1} + z_{t-2}) + \epsilon_t$
Sign Auto-Regressive process	$sign(x) = \begin{cases} 1 & \text{if } x > 0 \\ 0 & \text{for } x = 0 \\ -1 & \text{for } x < 0 \end{cases}$
Nonlinear Moving Average process	$NMA(2) : z_t = \epsilon_t - 0.3\epsilon_{t-1} + 0.2\epsilon_{t-2} + 0.4\epsilon_{t-1}\epsilon_{t-2} - 0.25\epsilon_{t-2}^2$
Nonlinear Auto-Regressive process	$NAR(2) : z_t = \frac{0.7 z_{t-1} }{ z_{t-1} +2} + \frac{0.35 z_{t-2} }{ z_{t-2} +2} + \epsilon_t$
Bilinear process	$BL(2) : z_t = 0.4z_{t-1} - 0.3z_{t-2} + 0.5z_{t-1}\epsilon_{t-1} + \epsilon_t$
Smooth Transition Auto-Regressive process	$STAR(2) : z_t = 0.3z_{t-1} + 0.6z_{t-2} + \frac{0.1 - 0.9z_{t-1} + 0.8z_{t-2}}{1 + e^{-10z_{t-1}}} + \epsilon_t$
Threshold Auto-Regressive process	$TAR(2) : z_t = \begin{cases} 0.9z_{t-1} + 0.05z_{t-2} + \epsilon_t & \text{for }  z_{t-1}  \leq 1 \\ -0.3z_{t-1} + 0.65z_{t-2} - \epsilon_t & \text{for }  z_{t-1}  > 1 \end{cases}$

Table 6: The DGPs used to simulate time series with random-walk behavior.

Process name	Process mathematical model
Trend Random-Walk process	$(TRW) : z_t = z_{t-1} + \epsilon_t$
Seasonal Random-Walk process	$(SRW) : z_t = z_{t-4} + \epsilon_t$
Trend and Seasonal Random-Walk process	$(TSRW) : z_t = z_{t-1} + z_{t-4} - z_{t-5} + \epsilon_t$

Table 7: The DGPs used to simulate time series with long-memory behavior.

Process name	Process mathematical model
$ARFIMA(p = 2, d = 0.2, q = 2)$	$z_t^{(0.2)} = 0.7z_{t-1}^{(0.2)} - 0.1z_{t-2}^{(0.2)} - 0.5\epsilon_{t-1} + 0.4\epsilon_{t-2} + \epsilon_t$
$ARFIMA(p = 2, d = 0.4, q = 2)$	$z_t^{(0.4)} = 0.7z_{t-1}^{(0.4)} - 0.1z_{t-2}^{(0.4)} - 0.5\epsilon_{t-1} + 0.4\epsilon_{t-2} + \epsilon_t$

Table 8: The DGPs used to simulate time series with chaotic behavior.

Process name	Process mathematical model
Mackey-Glass process	$\frac{dx}{dt} = a \frac{x(t-\tau)}{1+x^c(t-\tau)} - bx(t)$ such that $(\tau = 17, a = 0.2, b = 0.1, c = 10)$ (Ma et al. 2007)
Hénon-Map process	$x_{t+1} = 1 + y_t - ax^2$ ; $y_{t+1} = bx_t$ such that $(a = 1.4, b = 0.3)$ (Li & Lin 2016)
Rössler process	$\dot{x} = -y - z$ ; $\dot{y} = x + ay$ ; $\dot{z} = b + z(x - c)$ $(a = 0.15, b = 0.2, c = 10, x_0 = 10, y_0 = z_0 = 0)$ (Lim & Puthusserpady 2007)
Lorenz process	$\dot{x} = \sigma(y - x)$ ; $\dot{y} = -xz + rx - y$ ; $\dot{z} = xy - bz$ $(\sigma = 16, r = 45.92, b = 4, x_0 = y_0 = z_0 = 1)$ (Lim & Puthusserpady 2007)

### 5.2. RNN-cells used for experiments 1 and 2

To evaluate each cell structure with respect to each times series behavior, we conducted two experiments as summarized in Table 9. The first experiment evaluates LSTM-Vanilla and 11 of its variants created based on one alteration in the basic Vanilla architecture that consists of (1) removing, (2) adding, or (3) substituting one cell component (Table A.24): (1) The first three variants NIG (No Input Gate), NFG (No Forget Gate), and NOG (No Output Gate) were created through the deactivation of the input gate, the forget gate, and the output gate, respectively. The four subsequent variants NIAF (No Input Activation Function), NFAF (No Forget Activation Function), NOAF (No Output Activation Function), and NCAF (No Candidate Activation Function) were constructed through the elimination of the input, forget, output, and candidate activation function, respectively. (2) The two subsequent variants PC (Peephole Connections), and FGR (Full Gate Recurrence) were designed through the creation of new connections between the cell state and the gates, and between the current states and the previous states of the gates, respectively. (3) Eventually, FB1 (Forget Gate Bias 1) and CIFG (Coupled Input Forget Gate) was conceived by setting the forget gate bias to one, and by coupling the input and the forget gate into one gate, respectively.

The second experiment evaluates and analyzes the performance of 20 possible RNN-cell structures: JORDAN, ELMAN, MRNN, SCRNN, IRNN, LSTM-Vanilla, GRU, MGU, MUT1, MUT2, MUT3, and 9 SLIM

variants mapping LSTM, GRU, and MGU. A summary of the evaluated cells related to each experiment is presented in Table 9, and the cellular calculations inside each cell are presented in Table A.25.

Table 9: List of evaluated RNN models with regard to each experiment with their theoretic complexity, number of weight matrices, and number of bias vectors.  $n_I$  is the number of inputs,  $n_H$  is the number of hidden nodes,  $n_S$  is the number of context nodes, and  $n_O$  is the number of outputs.

RNN models					
	Short name	Full name	Theoretic complexity	# Weight matrices	# Bias vectors
Experiment 1	NIG	LSTM with No Input Gate	$3n_I n_H + 3n_H^2 + 3n_H$	6	3
	NFG	LSTM with No Forget Gate	$3n_I n_H + 3n_H^2 + 3n_H$	6	3
	NOG	LSTM with No Output Gate	$3n_I n_H + 3n_H^2 + 3n_H$	6	3
	CIFG	LSTM with Coupled Input Forget Gate	$3n_I n_H + 3n_H^2 + 3n_H$	6	3
	FB1	LSTM with Forget Gate Bias 1	$4n_I n_H + 4n_H^2 + 3n_H$	6	3
	NIAF	LSTM with No Input Activation Function	$4n_I n_H + 4n_H^2 + 4n_H$	8	4
	NFAF	LSTM with No Forget Activation Function	$4n_I n_H + 4n_H^2 + 4n_H$	8	4
	NOAF	LSTM with No Output Activation Function	$4n_I n_H + 4n_H^2 + 4n_H$	8	4
	NCAF	LSTM with No Candidate Activation Function	$4n_I n_H + 4n_H^2 + 4n_H$	8	4
	Vanilla	LSTM Vanilla	$4n_I n_H + 4n_H^2 + 4n_H$	8	4
	PC	LSTM with Peephole Connections	$4n_I n_H + 7n_H^2 + 4n_H$	11	4
	FGR	LSTM with Full Gate Recurrence	$4n_I n_H + 13n_H^2 + 4n_H$	17	4
Experiment 2	ELMAN	ELMAN	$n_I n_H + n_H^2 + n_H$	2	1
	IRNN	Identity Recurrent Neural Network	$n_I n_H + n_H^2 + n_H$	2	1
	JORDAN	JORDAN	$n_I n_H + n_O n_H + n_H$	2	1
	MRNN	Multi-Recurrent Neural Network	$n_I n_H + n_H^2 + n_O n_H + n_H$	3	1
	SCRN	Structurally Constrained Recurrent Network	$n_I n_S + n_I n_H + n_H^2 + n_S n_H + n_H$	4	1
	MGU-SLIM3	Minimal Gate Unit SLIM3	$n_I n_H + n_H^2 + 2n_H$	2	2
	MGU-SLIM2	Minimal Gate Unit SLIM2	$n_I n_H + 2n_H^2 + n_H$	3	1
	MGU-SLIM1	Minimal Gate Unit SLIM1	$n_I n_H + 2n_H^2 + 2n_H$	3	2
	MGU	Minimal Gate Unit	$2n_I n_H + 2n_H^2 + 2n_H$	4	2
	GRU-SLIM3	Gated Recurrent Unit SLIM3	$n_I n_H + n_H^2 + 3n_H$	2	3
	GRU-SLIM2	Gated Recurrent Unit SLIM2	$n_I n_H + 3n_H^2 + n_H$	4	1
	GRU-SLIM1	Gated Recurrent Unit SLIM1	$n_I n_H + 3n_H^2 + 3n_H$	4	3
	MUT1	Gated Recurrent Unit Mutation 1	$2n_I n_H + 2n_H^2 + 3n_H$	4	3
	MUT2	Gated Recurrent Unit Mutation 2	$2n_I n_H + 3n_H^2 + 3n_H$	5	3
	MUT3	Gated Recurrent Unit Mutation 3	$3n_I n_H + 3n_H^2 + 3n_H$	6	3
	GRU	Gated Recurrent Unit	$3n_I n_H + 3n_H^2 + 3n_H$	6	3
	LSTM-SLIM3	LSTM SLIM3	$n_I n_H + n_H^2 + 4n_H$	2	4
	LSTM-SLIM2	LSTM SLIM2	$n_I n_H + 4n_H^2 + n_H$	5	1
	LSTM-SLIM1	LSTM SLIM1	$n_I n_H + 4n_H^2 + 4n_H$	5	4
	LSTM-Vanilla	LSTM Vanilla	$4n_I n_H + 4n_H^2 + 4n_H$	8	4

The studied RNN cells have different degrees of complexity, which is referred to as theoretic complexity (Table 9). This complexity is defined by the number of parameters inside each cell which depends on the number of inputs, the number of hidden nodes, the number of context nodes (in the case of the SCRN model), and the number of outputs. During the hyperparameter tuning the complexity of the cell may increase or decrease depending on the optimal number of hidden nodes found. Thus, the complexity of the cell defined after the hyperparameter tuning is called empirical complexity.

### 5.3. Data preparation

Before starting the modeling process, each time series data was partitioned into three subsets: the first 2000 observations were used to train the models in order to find the best parameters, the next 500 observations were used to select the best configuration of hyperparameters of each model, and the last 500 observations were used to test the out-of-sample performance of these models (Figure 13). Each of these partitions was normalized, then converted from unstructured into structured data (Figure 14) by reshaping it based on the number of time steps  $T$  (estimation window size) and the number of horizons  $H$  (forecasting window size). Thus, we converted the raw time series data  $(Z_t)_{t \in \mathbb{N}} = (z_1, z_2, \dots, z_n)$  into a structured data  $S = \{(X^{(i)}, Y^{(i)}), i \in \{1, \dots, m\}\} = S_{train} \cup S_{validation} \cup S_{test}$ . Where  $X^{(i)} = (z_i, z_{(i+1)}, \dots, z_{(i+T-1)})$  and  $Y^{(i)} = (z_{(i+T)})$  because we are handling one-time-step-ahead forecasting.

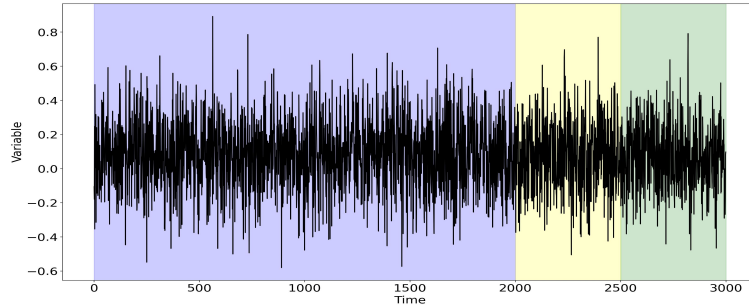


Figure 13: Visualization of data partitioning into a training set (purple color), validation set (yellow color), and test set (green color). The plotted time series is a sample of NMA process.

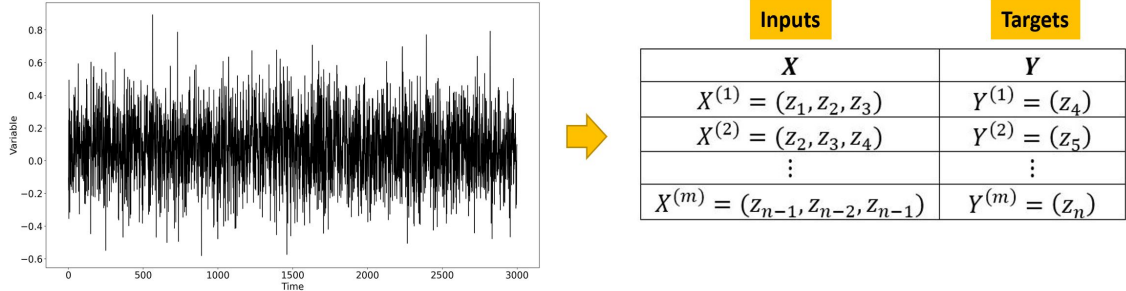


Figure 14: Visualization of data structuring from raw to tabular data. In this case, the number of time steps  $T = 3$  and the number of horizons  $H = 1$ .

### 5.4. Parameter optimization

To find the best set of parameters (weight  $W$  and bias  $b$ ), first, the model parameters were initialized by Kaiming method (He et al. 2015), then optimized using a stochastic gradient descent-based algorithm named Adam (Kingma & Ba 2014) (Algorithm 1) by minimizing the cost function  $J$  that describes a Mean

Square Error (MSE) using a mini-batch size of 100 (Table 10).

$$J = \frac{1}{|S_{train}|} \sum_{i=1}^{|S_{train}|} (Y^{(i)} - \hat{Y}^{(i)})^2$$

$$\hat{Y}^{(i)} = h_T \cdot W_{hy} + b_y$$

Where  $\hat{Y}^{(i)}$  is the predicted value of instance  $i$  computed using the identity output activation function,  $W_{hy}$  is the weight matrix between the hidden and the output layer, and  $b_y$  is the output layer bias.

---

**Algorithm 1** Description of the parameter optimization process using Adam algorithm.

---

**Require:** The learning rate  $\alpha = 0.01$

**Require:** The exponential decay rates for the moments estimates  $\beta_1 = 0.9$ ,  $\beta_2 = 0.999$ , and  $\epsilon = 10^{-8}$

**Require:** The cost function  $J$  with parameters  $W$  and  $b$  to be minimized.

- 1:  $V_{dW} = 0$ ,  $V_{db} = 0$ ,  $S_{dW} = 0$ , and  $S_{db} = 0$
  - 2: **for** each iteration  $t$  **do**
  - 3:   Compute the  $dW$  and  $db$ :
  - 4:    $dW = \frac{\partial J}{\partial W}$  and  $db = \frac{\partial J}{\partial b}$
  - 5:   Update the biased first moments estimates  $V_{dW}$  and  $V_{db}$ :
  - 6:    $V_{dW} \leftarrow \beta_1 V_{dW} + (1 - \beta_1) dW$  and  $V_{db} \leftarrow \beta_1 V_{db} + (1 - \beta_1) db$
  - 7:   Update the biased second moments estimates  $S_{dW}$  and  $S_{db}$ :
  - 8:    $S_{dW} \leftarrow \beta_2 S_{dW} + (1 - \beta_2) (dW)^2$  and  $S_{db} \leftarrow \beta_2 S_{db} + (1 - \beta_2) (db)^2$
  - 9:   Update the bias-corrected first moments estimates  $v_{dW}^{corr}$  and  $v_{db}^{corr}$ :
  - 10:    $v_{dW}^{corr} = \frac{V_{dW}}{(1 - \beta_1^t)}$  and  $v_{db}^{corr} = \frac{V_{db}}{(1 - \beta_1^t)}$
  - 11:   Update the bias-corrected second moments estimates  $S_{dW}^{corr}$  and  $S_{db}^{corr}$ :
  - 12:    $S_{dW}^{corr} = \frac{S_{dW}}{(1 - \beta_2^t)}$  and  $S_{db}^{corr} = \frac{S_{db}}{(1 - \beta_2^t)}$
  - 13:   Update the parameters  $W$  and  $b$ :
  - 14:    $W \leftarrow W - \alpha \times \frac{v_{dW}^{corr}}{\sqrt{S_{dW}^{corr}} + \epsilon}$  and  $b \leftarrow b - \alpha \times \frac{v_{db}^{corr}}{\sqrt{S_{db}^{corr}} + \epsilon}$
  - 15: **end for**
- 

### 5.5. Hyperparameter tuning

Within this section, we present the approach used to select the best architecture for each model. This architecture is defined by two hyperparameters: 1) the number of time steps  $T$ , and 2) The number of hidden neurons  $n_H$ . To find the best combination  $\{T, n_H\}$  we used a Grid Search algorithm (Algorithm 2) that loops over each possible combination in a grid created in two-dimensional space defined by  $T$  and  $n_H$ . The other hyperparameters such as the initial learning rate and the minibatch size were set based on the literature (Parmezan et al. 2019) (Table 10).

---

**Algorithm 2** Description of the hyperparameter tuning process.

---

```
1: Best_Error =  $+\infty$ 
2: Best_Config = None
3: for  $T$  in 1 to  $T_{max}$  do
4:   for  $n_H$  in 1 to  $n_{H_{max}}$  do
5:     Define an empty array Errors.
6:     for  $i$  in 1 to 10 do
7:       Train the model with the combination  $\{T, n_H\}$  using Algorithm 1.
8:       Compute the MSE of the model on the validation set.
9:       Append this error to the array Errors.
10:    end for
11:    Compute the average overall MSE values in the array Errors.
12:    if MSE < Best_Error then
13:      Best_Error = MSE
14:      Best_Config =  $\{T, n_H\}$ 
15:    end if
16:  end for
17: end for
```

---

Using each combination  $\{T, n_H\}$ , the model was trained ten times for a maximum number of 500 epochs in which we save the best set of parameters that minimizes the average MSE over the ten runs in the validation set (Algorithm 2). The objective behind this is to avoid the bias generated by the parameter initialization method and also to select the most stable model's architecture.

The maximum number  $n_{H_{max}}$  of evaluated hidden neurons is 10 because we are using univariate time series (Table 10), while the maximum number  $T_{max}$  of evaluated time steps is described in Table 11 for each behavior. To define  $T_{max}$  used in the chaotic time series, we used the values recommended by (Parmezan et al. 2019) since we used their chaotic datasets. In the long-memory behavior,  $T_{max}$  was selected based on the last relevant peak visualized in the ACF (Auto Correlation Function) graph and the PACF (Partial Auto Correlation Function) graph. In the Nonlinear behavior, we already know that the time series were generated with an order equal to 2, but in order to find the best number of time steps, we set  $T_{max} = 5$  for two reasons: 1) we need to simulate the fact that the model is not aware of the DGP, which is a mandatory condition to use machine learning models. 2) we cannot use the ACF and PACF tests in this case because they can only capture the linear correlations in the data, however, we are using nonlinear data which necessarily contains nonlinear correlations. In the deterministic behavior, we used  $T_{max} = 10$  for the T DGP, and  $T_{max} = 5$  for the remaining DGPs using the seasonality period. In the random-walk behavior, we used  $T_{max} = 5$  for the TSRW DGP,  $T_{max} = 4$  for the SRW DGP, and  $T_{max} = 10$  for the TRW DGP.

Table 10: The values of the hyperparameters used to train the studied RNN models.

Hyperparameter	Value
Mini-batch size	100
Maximum number of epochs	500
Learning rate $\alpha$	0.01
Optimization algorithm	Adam
Cost function	MSE
Horizon $H$	1
Maximum number of hidden neurons $n_{H\max}$	10

 Table 11: The  $T_{\max}$  values used for each DGP of each time series behavior.

Behavior	DGP	$T_{\max}$
Deterministic behavior	T	10
	SS	5
	CS	5
	TSS	5
	TCS	5
Random-walk behavior	TRW	10
	SRW	4
	TSRW	5
Nonlinear behavior	SAR(2)	5
	NMA(2)	5
	NAR(2)	5
	BL(2)	5
	STAR(2)	5
	TAR(2)	5
Long-memory behavior	ARFIMA(2, 0.2, 2)	20
	ARFIMA(2, 0.4, 2)	40
Chaotic behavior	Mackey-Glass	7
	Hénon map	3
	Rössler	14
	Lorenz	25

The hyperparameter tuning was performed using the first replicate for each DGP because changing the white noise generator to create these 30 replicates does not change the linear/nonlinear correlations in the time series, it only impacts the randomness of the data. Therefore, the combination  $T, n_H$  remains

appropriate for all the 30s replicates. In total, we performed 200 experiments for each model (Table 3) which sums up to 6200 experiments in the whole study. Once the best architecture of each model was found, the training and the validation sets were merged to form a new training set on which the best model's configuration is retrained for 500 epochs, then evaluated on the test set.

### 5.6. Performance evaluation

To evaluate the forecasting performance of the models, a set of statistical metrics were used. These statistical metrics together provide assistance to compare the models and select the best one. The used metrics are classified into four subsets:

- Error-based metrics: these metrics only measure the number of errors made by a predictive model by evaluating the goodness-of-fit of the model. Two metrics were used: the Mean Absolute Error (MAE) and the Root Mean Square Error (RMSE). The RMSE measures the standard deviation of residuals, it penalizes large errors. While the MAE measures the average magnitude of the residuals, it is less prone to outliers.

$$RMSE = \sqrt{\frac{1}{|S_{test}|} \sum_{i=1}^{|S_{test}|} (Y^{(i)} - \hat{Y}^{(i)})^2}$$

$$MAE = \frac{1}{|S_{test}|} \sum_{i=1}^{|S_{test}|} |Y^{(i)} - \hat{Y}^{(i)}|$$

- Information criterion-based metrics: these metrics deal with the trade-off between the goodness-of-fit of the model and the simplicity of the model. They penalize complex models by combining the number of errors committed by the model, the number of parameters (i.e., weights and biases) employed by the model to generate the output, and the sample size. They measure the amount of information lost by a model. A low value of these metrics implies less information loss, therefore high model quality. A set of five main statistical criteria were employed: Akaike Information Criterion (AIC) (Akaike 1969), Bayesian Information Criterion (BIC) (Findley 1991), Amemiya Prediction Criterion (APC) (Amemiya 1980), Hocking's Sp (HSP) (Hocking 1976), and Sawa's Bayesian Information Criterion (SBIC) (Sawa 1978).

$$AIC = |S_{test}| \ln\left(\frac{SSE}{|S_{test}|}\right) + 2K$$

$$BIC = |S_{test}| \ln\left(\frac{SSE}{|S_{test}|}\right) + K \ln(|S_{test}|)$$

$$APC = \frac{|S_{test}| + K}{|S_{test}|(|S_{test}| - K)} SSE$$

$$HSP = \frac{SSE}{|S_{test}|(|S_{test}| - K - 1)}$$

$$SBIC = |S_{test}| \ln\left(\frac{SSE}{|S_{test}|}\right) + 2(K + 2)q + 2q^2$$

$$q = |S_{test}| \frac{\sigma^2}{SSE}$$

Where  $SSE$  is the sum square error,  $K$  is the number of parameters used by the model (empirical complexity), and  $\sigma$  is the standard deviation of the prediction errors.

$$SSE = \sum_{i=1}^{|S_{test}|} (Y^{(i)} - \hat{Y}^{(i)})^2$$

- Naïve-based metric: this metric compares the performance of the predictive model with the naïve model. It is called Theil's U (TU) coefficient (Parmezan et al. 2019). The naïve model assumes that the best value at time  $t + 1$  is the value obtained at time  $t$ . The values of this metric can be interpreted based on different ranges as follows: if  $(TU > 1)$ , the model's performance is lower than the naïve model. If  $(TU = 1)$ , the model's performance is the same as the naïve model. If  $(TU < 1)$ , the model's performance is higher than the naïve model. If  $(TU <= 0.55)$ , the model is trusted to carry out future predictions.

$$TU = \frac{SSE}{\sum_{i=1}^{|S_{test}|} (Y^{(i)} - Y^{(i-1)})^2}$$

- Direction change-based metric: this metric is called Prediction Of Change In Direction (POCID) (Parmezan et al. 2019). It measures the accuracy in the direction changes. It accumulates, over time, the differences in the direction change between the predicted and the observed values. It penalizes the model when its direction change in the predicted values between two consecutive time steps ( $i - 1$  and  $i$ ) is different than those of the observed values. This metric is complementary to analyzing the prediction errors. A high value of this metric implies a high similarity degree in the direction changes between the predicted values and the observed values.

$$POCID = 100 \times \frac{1}{|S_{test}|} \sum_{i=1}^{|S_{test}|} D^{(i)}$$

$$D^{(i)} = \begin{cases} 1 & \text{if } (\hat{Y}^{(i)} - \hat{Y}^{(i-1)})(Y^{(i)} - Y^{(i-1)}) > 0 \\ 0 & \text{otherwise} \end{cases}$$

All the aforementioned metrics were computed by averaging their values over the 30 replicates of the test set of all the DGPs of one specific behavior.

Choosing the best model can be very challenging when different performance metrics are available. To facilitate this task, a new metric was created using the combination of all the aforementioned metrics. We call this metric Multi-Criteria Index Measure (MCIM). Unlike the error measures, which generate values that need to be minimized, the POCID index must be maximized. Therefore, a complement of the POCID was created called Error Rate (ER):

$$ER = 100 - POCID$$

Afterward, the MCIM metric was defined by computing the average over all the normalized values of the used metrics. The normalization was used because the performance metrics have different ranges of values. The normalization was performed using the Min-Max method.

$$MCIM(M) = \frac{1}{|S_{PI(M)}|} \sum_{i=1}^{|S_{PI(M)}|} PI_i^{(n)}(M)$$

$$S_{PI(M)} = \{MAE(M), RMSE(M), AIC(M), BIC(M), APC(M), HSP(M), SBIC(M), TU(M), ER(M)\}$$

$$PI_i^{(n)}(M) = \frac{PI_i(M) - PI_{i/S_M}^{(min)}}{PI_i(M) - PI_{i/S_M}^{(max)}}$$

Where  $S_{PI(M)}$  is the set of values of the Performance Indices of model  $M$ ,  $PI_i(M)$  is the performance index type  $i$  of model  $M$ , and  $PI_i^{(n)}(M)$  is its normalized value.

$$PI_{i/S_M}^{(min)} = \min\{PI_i(M) : M = 1, \dots, |S_M|\}$$

$$PI_{i/S_M}^{(max)} = \max\{PI_i(M) : M = 1, \dots, |S_M|\}$$

$S_M$  is the set of evaluated models,  $PI_{i/S_M}^{(min)}$  is the minimum value of the performance index type  $i$  over the set of evaluated models  $S_M$ , and  $PI_{i/S_M}^{(max)}$  is the maximum value of the performance index type  $i$  over the set of evaluated models  $S_M$ .

The created MCIM metric was employed to rank all the evaluated RNN architectures and to select the best RNN structure for each specific time series behavior. However, relying solely on the MCIM metric may not be statistically reliable to select the best model. To quantify the likelihood of a model being the most performing, to improve our confidence in the models' interpretation and selection, to compare the performance of the RNN models, and to further examine whether any observed difference is statistically significant or it is only due to noise or chance, statistical significance tests should be used.

The choice of these tests depends on (1) the prediction task (classification or regression), (2) the data distribution, and (3) whether the models are compared on the same data or not. In our case, (1) we are solving forecasting tasks which is a type of dynamical regression, (2) we assume that the distribution of our data is unknown, and (3) all the models are tested on the same data. Therefore, a regression non-parametric paired statistical test referred to as Friedman Wilcoxon-Holm signed-rank test <sup>1</sup> was used to detect pairwise significance.

First, the Friedman test (Friedman 1940) between each pair of models is performed with a significance level of 5% to reject the null hypothesis ( $p\text{-value} < 0.05$ ). The null hypothesis of this test states that the pair of models are similar. Then, a pairwise post-hoc analysis based on the Wilcoxon-Holm method (with Holm's alpha 5% correction) was used to compare the results (Benavoli et al. 2016, Wilcoxon 1992, Holm 1979, Garcia & Herrera 2008, Abdulkarim 2016). To visualize this pairwise comparison and to highlight the difference significance, a critical difference diagram proposed by (Demšar 2006) was generated where a thick horizontal line groups a set of RNN models that are not significantly different.

## 6. Results and discussion

In this section, we present the results of the two conducted experiments: (1) The first experiment consists of evaluating and analyzing the role of each component in the LSTM-Vanilla cell with respect to the five time series behaviors. The evaluated architectures were generated by removing (NIG, NFG, NOG, NIAF, NFAF, NOAF, and NCAF), adding (PC and FGR), or substituting (FB1 and CIFG) one cell component. (2) The second experiment aims at evaluating and analyzing the performance of a multitude of RNN cell structures available in the literature (JORDAN, ELMAN, MRNN, SCRNN, IRNN, LSTM-Vanilla, GRU, MGU, MUT1, MUT2, MUT3, and 9 SLIM variants) in forecasting the five behaviors.

### 6.1. Experiment 1: Utility analysis of LSTM cell components in forecasting time series behaviors.

The impact of each component (i.e., input gate, forget gate, output gate, coupled input-forget gate, input activation function, forget activation function, output activation function, candidate activation function, fixing the forget bias to 1, peephole connections, and full gate recurrence) on the performance of LSTM-Vanilla model for predicting the deterministic, random-walk, nonlinear, long-memory, and chaotic behaviors are presented in this section.

Tables 12 to 16 present the average results of the 10 used statistical metrics for each variant of the LSTM-Vanilla model run on the test set of the five types of time series behaviors. It can be noticed that the error-based metrics select models with low residual values, however, the information criterion-based

---

<sup>1</sup>This statistical test was performed using the framework <https://github.com/hfawaz/cd-diagram> re-adapted to test forecasting models

metrics tend to select less complex models with low forecasting errors. Based on the new proposed MCIM metric, the structure CIFG is the most adapted to forecast time series data with deterministic (Table 12) and random-walk (Table 13) behaviors. The NOG variant outperforms the other models in forecasting data with nonlinear behavior (Table 14). The NIG design is more adapted for data with long-memory behavior (Table 15). The Vanilla structure reveals the higher ability to forecast time series data with chaotic behavior (Table 16).

Figures 15 to 19 display the distribution of the TU and the POCID metrics over all the 12 LSTM variants for the five time series behaviors. In the deterministic behavior, all the models perform better than the naïve model for more than half of the used data (Figure 15a). The POCID levels of NIAF, NCAF, and FB1 are lower than the remaining models (Figure 15b). In the random-walk behavior, all the models perform less than the naïve model for more than half of the used time series data (Figure 16a). They have approximately the same POCID amounts (Figure 16b). Within the nonlinear and the long-memory behaviors, the models performed less than the naïve model only for a small number of time series data (Figures 17a and 18a). The POCID levels of all the models are almost similar (Figures 17b and 18b). With respect to the chaotic behavior, for more than half of the data, the models proved that they can be trusted to forecast such type of behavior (Figure 19a). Similarly, the POCID values of all the used models are almost equal (Figure 19b).

The direction changes of the predicted values are more similar to the ones of the real values (almost oscillating around 60%) with the deterministic, random-walk, nonlinear, and chaotic behaviors (Figures 15b, 16b, 17b, and 19b) than with the long-memory behavior where the values are only hovering around 40% (Figure 18b).

To strengthen our interpretation of the models' performances with respect to the five time series behaviors, Figure 20 outlines the results of the statistical significance test between the used models for each data behavior. For the deterministic behavior, the CIFG structure is statistically different than all the other models (Figure 20a). With the nonlinear behavior, the NOG variant is statistically better than the remaining models (Figure 20c). With respect to the random-walk behavior, the CIFG and the NOAF have almost the same rank (Figure 20b). The NIG followed by the CIFG achieved the best results with the long-memory behavior (Figure 20d). With the chaotic behavior, the NOG followed by the NIG are better ranked than the Vanilla model recommended by the MCIM value (Table 16), however, there is no statistical difference between them (Figure 20e). For this type of behavior, the NOG variants are the most recommended by the used statistical test.

Table 12: Test results of LSTM-Vanilla variants for time series data with deterministic behavior.

	MAE	RMSE	TU	AIC	BIC	APC	HSP	SBIC	POCID	MCIM	Rank
<b>Vanilla</b>	0,0388	0,0481	0,8116	-3150,71	-2004,37	0,0153	1,51E-05	-3188,35	75,38	0,2977	5
<b>NIG</b>	0,0422	0,0520	1,0026	-3400,56	-2985,30	0,0041	5,96E-06	-3420,66	74,38	0,2402	4
<b>NFG</b>	0,0387	0,0476	0,5384	-3523,56	-3046,95	0,0043	5,87E-06	-3534,18	73,01	0,1474	2
<b>NOG</b>	0,0419	0,0522	0,7274	-3450,51	-3024,54	0,0042	6,31E-06	-3470,50	73,52	0,2034	3
<b>NIAF</b>	0,0458	0,0561	1,2036	-3328,43	-2947,16	0,0047	6,86E-06	-3369,75	74,02	0,3109	6
<b>NFAF</b>	0,0721	0,0856	1,3043	-2831,01	-2095,88	0,0195	2,51E-05	-2858,21	65,73	0,7793	12
<b>NOAF</b>	0,0403	0,0498	1,0145	-3213,70	-2207,87	0,0131	1,35E-05	-3283,54	75,10	0,3122	7
<b>NCAF</b>	0,0676	0,0785	0,9632	-2872,99	-1914,63	0,0170	2,23E-05	-2922,57	66,29	0,6689	11
<b>CIFG</b>	<b>0,0371</b>	<b>0,0459</b>	<b>0,6321</b>	<b>-3577,16</b>	<b>-3179,44</b>	<b>0,0032</b>	<b>4,76E-06</b>	<b>-3591,33</b>	<b>74,13</b>	<b>0,1210</b>	<b>1</b>
<b>FB1</b>	0,0660	0,0767	0,7920	-2961,69	-2089,54	0,0229	2,71E-05	-2981,35	66,52	0,6504	10
<b>PC</b>	0,0462	0,0573	1,2132	-3126,17	-2292,59	0,0092	1,10E-05	-3162,30	71,88	0,4111	8
<b>FGR</b>	0,0445	0,0549	1,0311	-1900,89	1991,09	-0,0142	-8,3E-06	-2152,23	71,43	0,4990	9

Table 13: Test results of LSTM-Vanilla variants for time series data with random-walk behavior.

	MAE	RMSE	TU	AIC	BIC	APC	HSP	SBIC	POCID	MCIM	Rank
<b>Vanilla</b>	0,0287	0,0347	35,4234	-3379,26	-1698,17	0,0088	8,84E-06	-3619,74	65,59	0,4714	11
<b>NIG</b>	0,0289	0,0353	24,8229	-3873,56	-3219,36	0,0044	5,05E-06	-3946,55	65,36	0,3121	5
<b>NFG</b>	0,0291	0,0347	18,9766	-3890,46	-3194,67	0,0034	4,15E-06	-4028,81	64,94	0,3151	6
<b>NOG</b>	0,0273	0,0329	20,1432	-4110,57	-3687,67	0,0026	3,71E-06	-4161,53	65,15	0,2176	4
<b>NIAF</b>	0,0369	0,0438	352,6018	-3399,64	-2086,53	0,0178	1,97E-05	-3610,75	64,15	0,8970	12
<b>NFAF</b>	0,0279	0,0336	29,0595	-3684,21	-2632,86	0,0033	3,96E-06	-3821,16	64,80	0,3747	8
<b>NOAF</b>	0,0252	0,0310	13,0473	-4227,70	-3977,46	0,0015	2,34E-06	-4251,86	65,49	0,1193	2
<b>NCAF</b>	0,0271	0,0326	22,9176	-3659,89	-2394,30	0,0044	4,81E-06	-3816,47	64,76	0,3833	9
<b>CIFG</b>	<b>0,0234</b>	<b>0,0285</b>	<b>15,1138</b>	<b>-4290,79</b>	<b>-3993,92</b>	<b>0,0013</b>	<b>1,94E-06</b>	<b>-4324,71</b>	<b>65,33</b>	<b>0,0830</b>	<b>1</b>
<b>FB1</b>	0,0259	0,0314	47,4964	-3954,61	-3213,19	0,0025	3,30E-06	-4044,93	65,68	0,2090	3
<b>PC</b>	0,0254	0,0309	28,5131	-3573,45	-1977,54	0,0086	8,24E-06	-3747,50	64,91	0,4238	10
<b>FGR</b>	0,0213	0,0259	13,2219	-3094,99	104,24	-0,0011	-2,00E-07	-3497,19	65,17	0,3705	7

Table 14: Test results of LSTM-Vanilla variants for time series data with nonlinear behavior.

	MAE	RMSE	TU	AIC	BIC	APC	HSP	SBIC	POCID	MCIM	Rank
<b>Vanilla</b>	0,1147	0,1437	0,5826	-1820,62	-626,42	0,0704	7,81E-05	-1852,35	55,58	0,5189	11
<b>NIG</b>	0,1142	0,1430	0,5787	-1977,20	-1110,66	0,0517	6,19E-05	-2003,20	55,57	0,3706	4
<b>NFG</b>	0,1138	0,1424	0,5739	-1897,99	-845,29	0,0505	6,06E-05	-1921,56	54,56	0,4039	6
<b>NOG</b>	<b>0,1135</b>	<b>0,1420</b>	<b>0,5677</b>	<b>-2148,56</b>	<b>-1645,13</b>	<b>0,0380</b>	<b>5,01E-05</b>	<b>-2163,75</b>	<b>55,05</b>	<b>0,2187</b>	<b>1</b>
<b>NIAF</b>	0,1140	0,1428	0,5756	-1977,74	-1104,28	0,0586	6,76E-05	-2001,51	55,16	0,3853	5
<b>NFAF</b>	0,1141	0,1428	0,5766	-1952,86	-1026,12	0,0553	6,49E-05	-1981,19	54,88	0,4139	7
<b>NOAF</b>	0,1159	0,1458	0,5891	-2006,59	-1243,99	0,0593	6,94E-05	-2022,09	54,28	0,6649	12
<b>NCAF</b>	0,1140	0,1430	0,5812	-2092,99	-1492,28	0,0392	5,14E-05	-2108,14	54,74	0,3658	3
<b>CIFG</b>	0,1155	0,1448	0,5943	-2045,55	-1368,08	0,0425	5,47E-05	-2059,41	56,04	0,4845	9
<b>FB1</b>	0,1136	0,1422	0,57	-1978,25	-1101,31	0,0415	5,30E-05	-1991,78	55,12	0,2922	2
<b>PC</b>	0,1141	0,1430	0,5834	-1829,74	-648,40	0,0707	7,80E-05	-1858,75	55,29	0,4878	10
<b>FGR</b>	0,1144	0,1430	0,5747	-1034,40	1910,12	-0,0410	-1,50E-05	-1110,85	55,34	0,4773	8

Table 15: Test results of LSTM-Vanilla variants for time series data with long-memory behavior.

	MAE	RMSE	TU	AIC	BIC	APC	HSP	SBIC	POCID	MCIM	Rank
<b>Vanilla</b>	0,0834	0,1046	0,8042	-2311,82	-1517,30	0,0312	3,66E-05	-2311,27	42,63	0,2158	8
<b>NIG</b>	<b>0,0819</b>	<b>0,1026</b>	<b>0,7767</b>	<b>-2563,29</b>	<b>-2349,46</b>	<b>0,0128</b>	<b>2,04E-05</b>	<b>-2559,39</b>	<b>42,13</b>	<b>0,0851</b>	<b>1</b>
<b>NFG</b>	0,0825	0,1033	0,7882	-2299,99	-1378,39	0,0251	3,04E-05	-2304,08	42,05	0,2593	10
<b>NOG</b>	0,0826	0,1035	0,7880	-2417,51	-1981,24	0,0168	2,42E-05	-2415,43	42,77	0,1298	4
<b>NIAF</b>	0,0834	0,1075	0,9296	-2470,59	-2174,63	0,0158	2,47E-05	-2467,95	42,20	0,1412	5
<b>NFAF</b>	0,0831	0,1042	0,8014	-2250,91	-1382,01	0,0228	2,92E-05	-2252,96	43,11	0,2147	7
<b>NOAF</b>	0,1002	0,2860	139,2791	-2059,28	-1192,65	3,2133	4,24E-03	-2061,37	43,42	0,8308	12
<b>NCAF</b>	0,0832	0,1045	0,8031	-2016,45	-503,06	0,0866	8,33E-05	-2023,55	42,67	0,3962	11
<b>CIFG</b>	0,0819	0,1026	0,7775	-2561,35	-2259,12	0,0133	2,06E-05	-2557,83	42,20	0,0868	2
<b>FB1</b>	0,0819	0,1026	0,7759	-2466,48	-2043,20	0,0152	2,24E-05	-2463,62	42,51	0,1179	3
<b>PC</b>	0,0831	0,1044	0,8033	-2355,37	-1579,13	0,0256	3,11E-05	-2354,66	41,73	0,2516	9
<b>FGR</b>	0,0823	0,1032	0,7862	-2380,71	-1746,97	0,0182	2,49E-05	-2381,48	42,19	0,1947	6

Table 16: Test results of LSTM-Vanilla variants for time series data with chaotic behavior.

	MAE	RMSE	TU	AIC	BIC	APC	HSP	SBIC	POCID	MCIM	Rank
<b>Vanilla</b>	<b>0,0532</b>	<b>0,0671</b>	<b>0,4772</b>	<b>-3475,04</b>	<b>-2677,35</b>	<b>0,0506</b>	<b>4,94E-05</b>	<b>-3486,80</b>	<b>59,06</b>	<b>0,2131</b>	<b>1</b>
<b>NIG</b>	0,0530	0,0669	0,5168	-3576,95	-3005,20	0,0089	1,38E-05	-3598,77	57,33	0,2299	2
<b>NFG</b>	0,0536	0,0677	0,5595	-3505,32	-2986,05	0,0139	1,81E-05	-3519,26	57,15	0,3227	7
<b>NOG</b>	0,0536	0,0676	0,5264	-3580,20	-3025,62	0,0178	2,15E-05	-3588,31	58,15	0,2355	3
<b>NIAF</b>	0,0622	0,0777	0,5529	-3497,35	-2960,94	0,0194	2,49E-05	-3510,89	57,34	0,5260	10
<b>NFAF</b>	0,0543	0,0695	0,5207	-3337,37	-2202,66	0,0622	6,01E-05	-3365,92	59,59	0,3263	8
<b>NOAF</b>	0,0529	0,0668	0,5287	-3300,57	-2173,95	0,0159	1,96E-05	-3363,36	57,58	0,2937	4
<b>NCAF</b>	0,0533	0,0673	0,5460	-3370,83	-2296,95	0,0168	2,05E-05	-3416,97	57,74	0,3071	5
<b>CIFG</b>	0,0561	0,0709	0,5346	-3446,18	-2694,20	0,0205	2,43E-05	-3466,81	58,58	0,3183	6
<b>FB1</b>	0,0602	0,0752	0,5673	-3166,73	-1891,64	0,0280	3,16E-05	-3216,24	58,15	0,5341	11
<b>PC</b>	0,0602	0,0752	0,5740	-3274,88	-2191,16	0,0808	7,64E-05	-3327,35	57,33	0,6630	12
<b>FGR</b>	0,0531	0,0669	0,4978	-1807,35	2662,05	-0,0312	-2E-05	-1992,26	58,40	0,4144	9

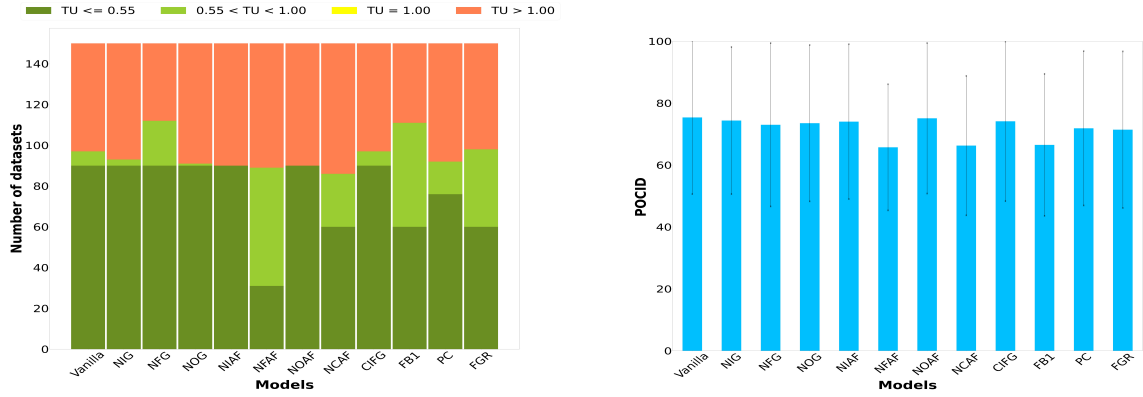


Figure 15: TU and POCID test results obtained by LSTM-Vanilla structures on deterministic time series.

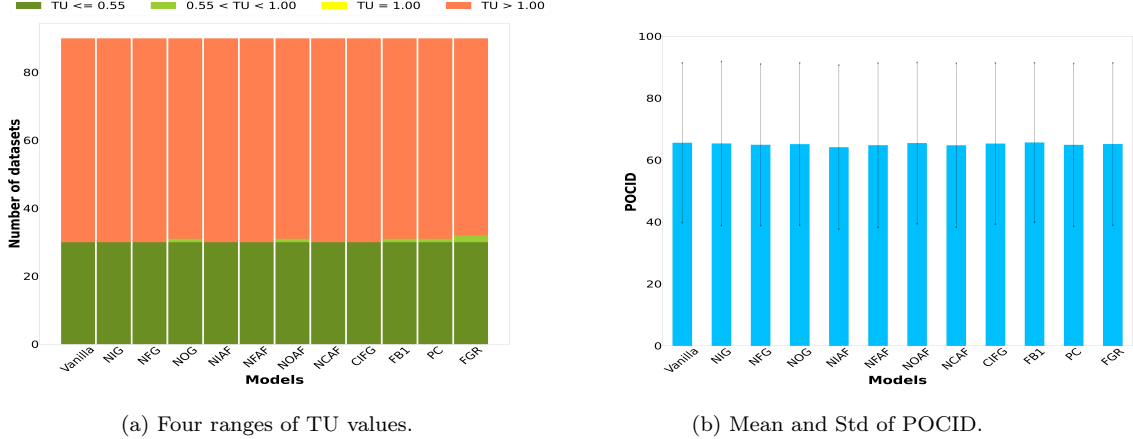


Figure 16: TU and POCID test results obtained by LSTM-Vanilla structures on random-walk time series

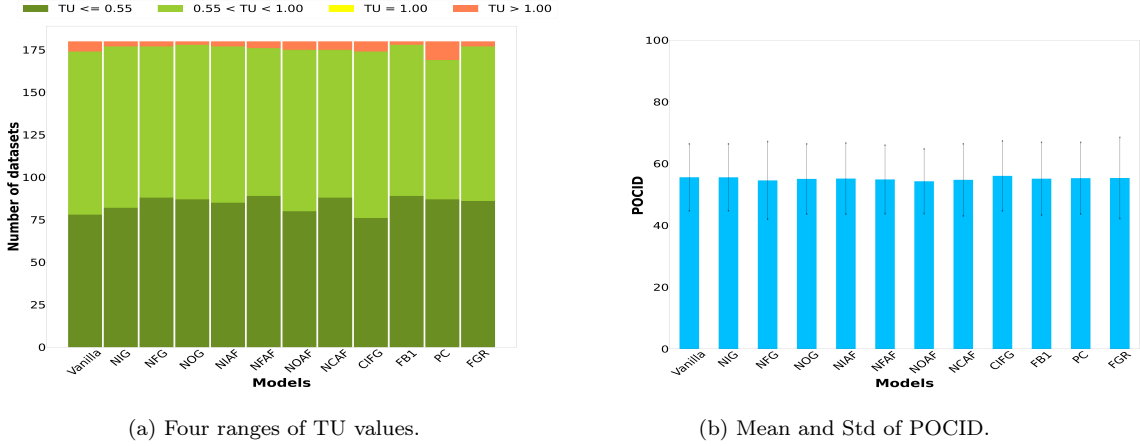


Figure 17: TU and POCID test results obtained by LSTM-Vanilla structures on nonlinear time series

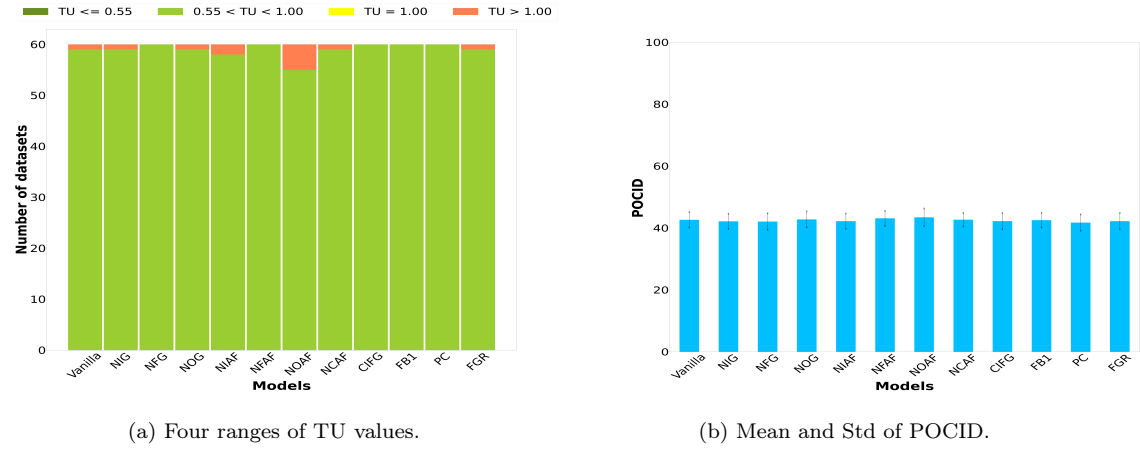


Figure 18: TU and POCID test results obtained by LSTM-Vanilla structures on long-memory time series

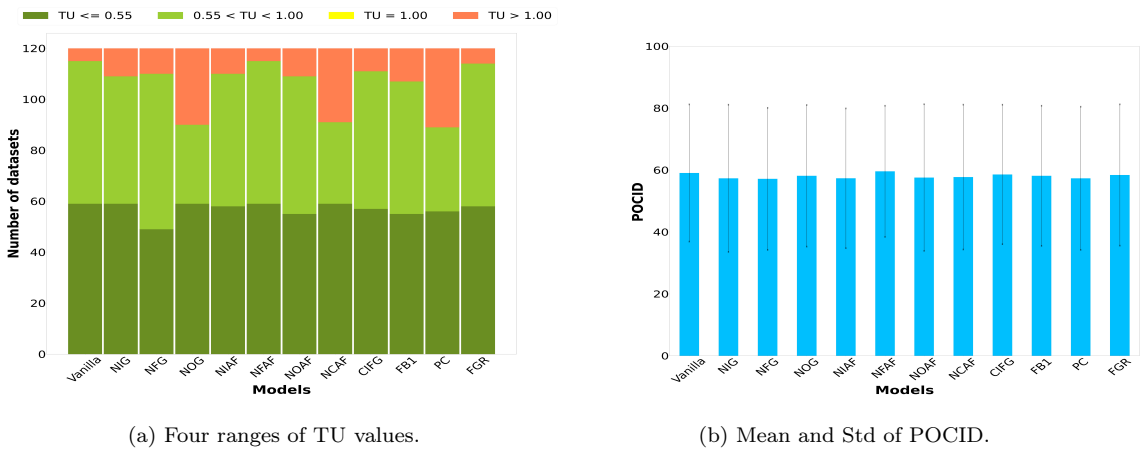
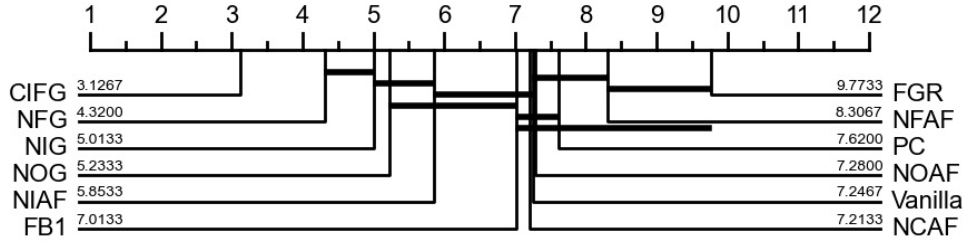
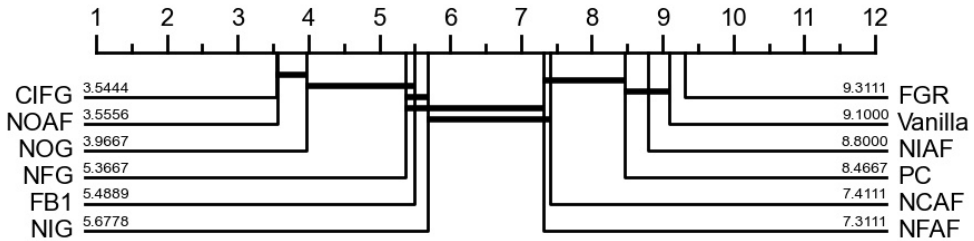


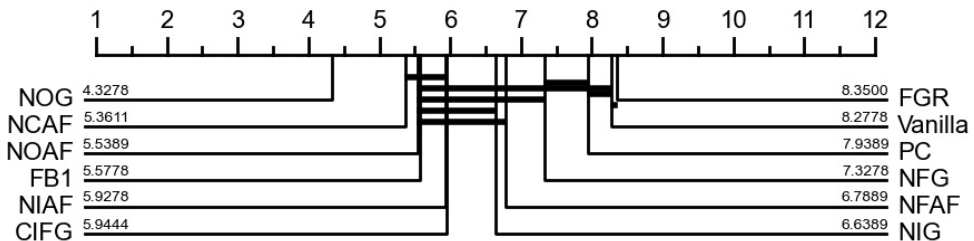
Figure 19: TU and POCID test results obtained by LSTM-Vanilla structures on chaotic time series



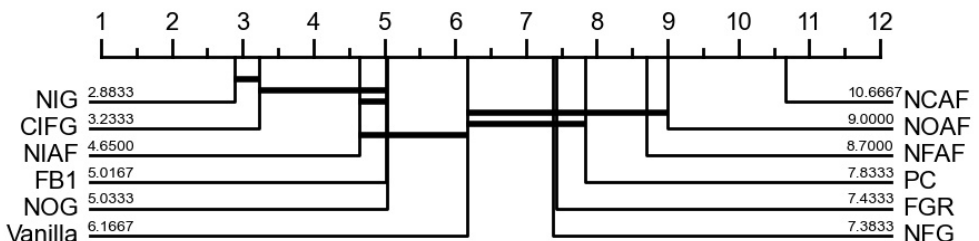
(a) Deterministic behavior.



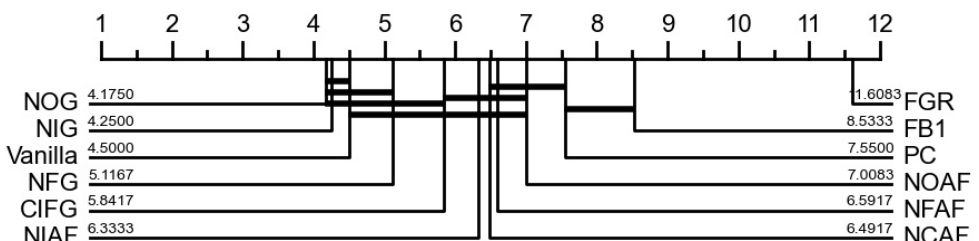
(b) Random-walk behavior.



(c) Nonlinear behavior.



(d) Long-memory behavior.



(e) Chaotic behavior.

Figure 20: CD diagrams for the MCIM values comparing the LSTM-Vanilla cell structures on the five time series behaviors.

## 6.2. Experiment 2: Performance analysis of different RNN cell structures in forecasting time series behaviors.

The performance of each RNN cell structure (JORDAN, ELMAN, MRNN, SCRNN, IRNN, LSTM-Vanilla, GRU, MGU, MUT1, MUT2, MUT3, and 9 SLIM variants) for predicting the deterministic behavior, random-walk behavior, nonlinear behavior, long-memory behavior, and chaotic behavior is provided in this section.

Tables 17 to 21 highlight the outcomes of the statistical metrics for each RNN model run on the five types of time series behaviors. Based on our MCIM metric, the model MGU-SLIM3 outperforms the other models with respect to the deterministic (Table 17) and the nonlinear (Table 19) behaviors. MGU-SLIM2 achieves better results than the remaining models when applied to data with random-walk (Table 18) and long-memory (Table 20) behaviors. Eventually, LSTM-SLIM3 exhibits higher abilities to forecast time series data with chaotic behavior (Table 21).

Figures 21 to 25 show the distribution of the TU and the POCID metrics over all the 20 RNN structures for the five time series behaviors. In the deterministic behavior, all the models perform better than the naïve model for more than half of the used data except the JORDAN model (Figure 21a). The models display different POCID levels but generally oscillate around 60% (Figure 21b). In the random-walk behavior, all the models perform less than the naïve model for more than half of the used time series data (Figure 22a). The basic RNN variants (ELMAN, JORDAN, MRNN, and IRNN) have smaller POCID values (less than 60%) compared to the other models (Figure 22b). With regard to the nonlinear and the long-memory behaviors, the models are performing widely better than the naïve model (Figures 23a and 24a). These models proved that they can be trusted to forecast nonlinear data for more than half of the time series. There are small variations in the POCID levels of these RNN models (Figures 23b and 24b). For the chaotic behavior, the RNN models are better than the naïve model for more than half of the time series data (Figure 25a). Similarly, there are small variations in the POCID levels of the RNN models (Figure 25b).

The direction changes of the predicted values are less similar to the ones of the real values for the long-memory behavior (oscillating around 40%) (Figure 24b), however, they are more similar to the remaining behaviors with a percentage more than 50% (Figures 21b, 22b, 23b, and 25b).

Figure 26 displays the statistical significance test results for top the 10 ranked models with respect to the five behaviors. With the deterministic behavior, the MUT2 followed by MGU, MGU-SLIM3, and GRU-SLIM3 are statistically similar such that the MUT2 variant is better ranked than the other models (Figure 26a). With the random-walk behavior, all the 10 models are statistically similar such that SCRNN followed by MGU-SLIM2 have the higher ranks (Figure 26b). For the nonlinear behavior, ELMAN is the top one ranked model that is significantly different than the remaining models (Figure 26c). This outcome appears to be different than the one presented in Table 19 where this model has the rank of five. For the long-memory behavior, MGU-SLIM2 and GRU-SLIM2 have similar ranks (Figure 26d, while LSTM-SLIM3 is the best-ranked model for the chaotic behavior (Figure 26e).

Table 17: Test results of RNN variants for time series data with deterministic behavior.

	MAE	RMSE	TU	AIC	BIC	APC	HSP	SBIC	POCID	MCIM	Rank
<b>ELMAN</b>	0,0777	0,0929	2,0477	-2983,50	-2935,19	0,0115	1,90E-05	-2979,17	66,07	0,7339	18
<b>JORDAN</b>	0,0794	0,0922	1,0851	-3089,27	-3021,59	0,0134	2,14E-05	-3085,68	61,10	0,6794	17
<b>MRNN</b>	0,0594	0,0717	1,0088	-3262,12	-3209,41	0,0066	1,09E-05	-3258,36	65,70	0,3971	14
<b>IRNN</b>	0,0880	0,1015	0,9632	-2951,90	-2734,79	0,0189	2,80E-05	-2951,70	57,48	0,8617	20
<b>SCRN</b>	0,0699	0,0827	0,7725	-3226,38	-3061,21	0,0125	1,93E-05	-3225,90	61,95	0,5492	16
<b>MUT1</b>	0,0403	0,0499	0,9056	-3403,41	-2826,57	0,0045	6,20E-06	-3436,33	71,53	0,2116	9
<b>MUT2</b>	0,0376	0,0465	0,6510	-3679,50	-3480,23	0,0029	4,64E-06	-3689,98	72,17	0,0276	3
<b>MUT3</b>	0,0438	0,0539	0,8292	-3359,13	-2631,38	0,0069	9,30E-06	-3405,58	68,53	0,2974	11
<b>MGU</b>	0,0373	0,0463	0,7275	-3651,80	-3441,96	0,0031	4,61E-06	-3655,85	73,17	0,0391	4
<b>MGU-SLIM1</b>	0,0714	0,0849	1,0354	-2984,17	-2428,10	0,0172	2,34E-05	-2991,50	63,83	0,7370	19
<b>MGU-SLIM2</b>	0,0373	0,0463	0,7616	-3522,46	-2994,61	0,0037	5,22E-06	-3558,84	74,67	0,1081	5
<b>MGU-SLIM3</b>	<b>0,0368</b>	<b>0,0455</b>	<b>0,7064</b>	<b>-3667,28</b>	<b>-3410,10</b>	<b>0,0031</b>	<b>4,62E-06</b>	<b>-3675,18</b>	<b>74,63</b>	<b>0,0232</b>	<b>1</b>
<b>GRU</b>	0,0413	0,0512	0,8014	-3517,85	-3102,46	0,0067	8,54E-06	-3531,20	70,88	0,1865	6
<b>GRU-SLIM1</b>	0,0381	0,0475	0,6157	-3390,80	-2634,37	0,0055	6,83E-06	-3423,60	72,53	0,2018	8
<b>GRU-SLIM2</b>	0,0486	0,0602	1,1913	-3371,85	-3088,15	0,0066	9,52E-06	-3381,21	69,68	0,3075	12
<b>GRU-SLIM3</b>	0,0368	0,0456	0,6022	-3676,72	-3403,73	0,0031	4,75E-06	-3689,67	72,39	0,0270	2
<b>LSTM-Vanilla</b>	0,0388	0,0481	0,8116	-3150,71	-2004,37	0,0153	1,51E-05	-3188,35	75,38	0,4291	15
<b>LSTM-SLIM1</b>	0,0424	0,0529	0,8197	-3433,15	-3024,88	0,0066	8,48E-06	-3441,72	72,09	0,2172	10
<b>LSTM-SLIM2</b>	0,0499	0,0606	0,8998	-3291,78	-2807,97	0,0060	9,19E-06	-3320,51	69,46	0,3268	13
<b>LSTM-SLIM3</b>	0,0428	0,0531	1,1304	-3447,89	-3153,68	0,0041	6,22E-06	-3458,40	73,50	0,1910	7

Table 18: Test results of RNN variants for time series data with random-walk behavior.

	MAE	RMSE	TU	AIC	BIC	APC	HSP	SBIC	POCID	MCIM	Rank
<b>ELMAN</b>	0,0928	0,1097	21,3471	-3285,91	-3246,38	0,0250	4,15E-05	-3287,33	56,51	0,7287	18
<b>JORDAN</b>	0,1020	0,1184	14,0806	-3320,03	-3274,63	0,0309	5,14E-05	-3321,53	48,45	0,8188	19
<b>MRNN</b>	0,0931	0,1105	66,4363	-3308,72	-3203,50	0,0296	4,82E-05	-3316,88	56,69	0,8471	20
<b>IRNN</b>	0,0839	0,0997	10,9240	-3549,6	-3430,98	0,0244	3,82E-05	-3560,61	56,14	0,6121	17
<b>SCRN</b>	0,0262	0,0314	17,7274	-4300,43	-4178,95	0,0015	2,35E-06	-4315,80	68,48	0,0361	2
<b>MUT1</b>	0,0333	0,0395	29,6909	-3824,18	-3339,95	0,0032	4,44E-06	-3895,82	65,42	0,2377	15
<b>MUT2</b>	0,0257	0,0308	15,3731	-4031,30	-3328,85	0,0027	3,36E-06	-4114,86	65,62	0,1395	12
<b>MUT3</b>	0,0245	0,0293	24,1815	-4098,09	-3570,16	0,0021	2,7E-06	-4148,32	65,94	0,1266	10
<b>MGU</b>	0,0263	0,0317	16,2492	-4005,74	-3476,69	0,0022	2,92E-06	-4062,89	66,98	0,1340	11
<b>MGU-SLIM1</b>	0,0236	0,0285	10,9444	-4227,87	-3840,13	0,0015	2,07E-06	-4265,43	65,07	0,0615	3
<b>MGU-SLIM2</b>	<b>0,0235</b>	<b>0,0282</b>	<b>13,5910</b>	<b>-4352,39</b>	<b>-4070,08</b>	<b>0,0013</b>	<b>2,03E-06</b>	<b>-4382,87</b>	<b>65,59</b>	<b>0,0276</b>	<b>1</b>
<b>MGU-SLIM3</b>	0,0262	0,0315	11,6589	-4185,93	-3995,77	0,0015	2,31E-06	-4208,46	65,44	0,0722	5
<b>GRU</b>	0,0235	0,0284	17,0903	-3958,84	-2981,02	0,0029	3,36E-06	-4062,29	65,15	0,1686	13
<b>GRU-SLIM1</b>	0,0242	0,0294	16,5218	-4250,87	-3986,04	0,0013	2,02E-06	-4286,01	64,89	0,0639	4
<b>GRU-SLIM2</b>	0,0252	0,0303	27,3054	-4219,19	-3933,82	0,0014	2,15E-06	-4260,82	66,44	0,0880	7
<b>GRU-SLIM3</b>	0,0250	0,03	10,2584	-4174,49	-3886,43	0,0014	2,08E-06	-4205,25	65,17	0,0729	6
<b>LSTM-Vanilla</b>	0,0287	0,0347	35,4234	-3379,26	-1698,17	0,0088	8,84E-06	-3619,74	65,59	0,4147	16
<b>LSTM-SLIM1</b>	0,0258	0,0315	12,9594	-3756,65	-2601,97	0,0056	5,77E-06	-3900,54	65,35	0,2364	14
<b>LSTM-SLIM2</b>	0,0255	0,0307	21,5779	-4090,69	-3601,71	0,0016	2,30E-06	-4160,11	65,66	0,1216	9
<b>LSTM-SLIM3</b>	0,0269	0,0322	19,3579	-4164,58	-3898,25	0,0017	2,56E-06	-4194,03	65,48	0,0984	8

Table 19: Test results of RNN variants for time series data with nonlinear behavior.

	MAE	RMSE	TU	AIC	BIC	APC	HSP	SBIC	POCID	MCIM	Rank
<b>ELMAN</b>	0,1149	0,1437	0,5812	-2340,32	-2281,75	0,0231	3,80E-05	-2336,61	52,67	0,1635	5
<b>JORDAN</b>	0,1178	0,1480	0,6117	-2279,52	-2187,23	0,0248	4,01E-05	-2277,59	48,36	0,4874	18
<b>MRNN</b>	0,1146	0,1436	0,5928	-2311,45	-2205,32	0,0241	3,87E-05	-2309,68	54,07	0,1830	7
<b>IRNN</b>	0,1151	0,1442	0,5844	-2268,78	-2054,90	0,0273	4,14E-05	-2272,43	51,28	0,2699	12
<b>SCRN</b>	0,1156	0,1441	0,6068	-2260,90	-2025,20	0,0275	4,22E-05	-2263,39	54,61	0,2932	14
<b>MUT1</b>	0,1133	0,1417	0,5671	-2260,10	-1992,21	0,0274	4,10E-05	-2265,44	55,08	0,0912	2
<b>MUT2</b>	0,1135	0,1420	0,5684	-2131,19	-1579,99	0,0362	4,86E-05	-2143,82	55,42	0,2234	8
<b>MUT3</b>	0,1145	0,1432	0,5783	-2056,78	-1359,81	0,0523	6,25E-05	-2080,26	53,34	0,4447	16
<b>MGU</b>	0,114	0,1428	0,5800	-2149,52	-1668,03	0,0311	4,45E-05	-2157,48	55,08	0,2463	10
<b>MGU-SLIM1</b>	0,1136	0,1422	0,5716	-2138,20	-1603,70	0,0320	4,50E-05	-2148,80	53,48	0,2433	9
<b>MGU-SLIM2</b>	0,1136	0,1422	0,5707	-2229,20	-1904,99	0,0296	4,31E-05	-2236,35	54,53	0,1549	4
<b>MGU-SLIM3</b>	<b>0,1130</b>	<b>0,1415</b>	<b>0,5662</b>	<b>-2261,98</b>	<b>-1997,78</b>	<b>0,0262</b>	<b>4E-05</b>	<b>-2264,52</b>	<b>54,55</b>	<b>0,0813</b>	<b>1</b>
<b>GRU</b>	0,1140	0,1428	0,5805	-1966,17	-1085,15	0,0420	5,36E-05	-1978,43	55,60	0,4098	15
<b>GRU-SLIM1</b>	0,1143	0,1430	0,5794	-2166,31	-1725,81	0,0313	4,47E-05	-2174,54	54,75	0,2506	11
<b>GRU-SLIM2</b>	0,1147	0,1436	0,5786	-2207,72	-1860,93	0,0339	4,72E-05	-2217,78	52,45	0,2890	13
<b>GRU-SLIM3</b>	0,1134	0,1418	0,5681	-2251,09	-1971,54	0,0262	4,01E-05	-2252,97	54,31	0,1115	3
<b>LSTM-Vanilla</b>	0,1147	0,1437	0,5826	-1820,62	-626,42	0,0704	7,81E-05	-1852,35	55,58	0,6735	20
<b>LSTM-SLIM1</b>	0,1137	0,1424	0,5756	-1925,86	-942,15	0,0547	6,42E-05	-1945,69	54,76	0,4806	17
<b>LSTM-SLIM2</b>	0,1140	0,1425	0,5699	-1890,03	-822,17	0,0688	7,62E-05	-1919,24	54,37	0,5702	19
<b>LSTM-SLIM3</b>	0,1138	0,1424	0,5678	-2277,20	-2064,31	0,0262	4,03E-05	-2279,11	50,25	0,1730	6

Table 20: Test results of RNN variants for time series data with long-memory behavior.

	MAE	RMSE	TU	AIC	BIC	APC	HSP	SBIC	POCID	MCIM	Rank
<b>ELMAN</b>	0,0831	0,1041	0,7994	-2613,9	-2376,66	0,0139	2,10E-05	-2609,74	40,36	0,1422	10
<b>JORDAN</b>	0,0879	0,1100	0,8836	-2606,64	-2540,76	0,0134	2,19E-05	-2601,62	36,50	0,2931	14
<b>MRNN</b>	0,0952	0,1189	1,2506	-2445,10	-2219,43	0,0178	2,75E-05	-2441,99	43,74	0,5397	19
<b>IRNN</b>	0,0875	0,1095	0,8701	-2597,71	-2435,18	0,0139	2,21E-05	-2593,91	37,10	0,2889	13
<b>SCRN</b>	0,0829	0,1039	0,7958	-2666,62	-2548,06	0,0121	1,95E-05	-2661,75	40,95	0,0738	4
<b>MUT1</b>	0,0834	0,1043	0,8052	-2618,77	-2526,96	0,0120	1,99E-05	-2613,97	39,67	0,1259	8
<b>MUT2</b>	0,0829	0,1038	0,7943	-2573,52	-2239,69	0,0140	2,10E-05	-2570,23	40,41	0,1632	11
<b>MUT3</b>	0,0844	0,1064	0,8395	-2142,53	-1053,80	0,0288	3,46E-05	-2144,50	43,41	0,5989	20
<b>MGU</b>	0,0818	0,1025	0,7749	-2575,53	-2427,40	0,0122	1,99E-05	-2570,85	42,02	0,0850	5
<b>MGU-SLIM1</b>	0,0823	0,1032	0,7870	-2488,92	-1997,73	0,0158	2,27E-05	-2487,78	42,37	0,1973	12
<b>MGU-SLIM2</b>	<b>0,0819</b>	<b>0,1026</b>	<b>0,7772</b>	<b>-2642,25</b>	<b>-2519,68</b>	<b>0,0119</b>	<b>1,94E-05</b>	<b>-2637,50</b>	<b>42,18</b>	<b>0,0438</b>	<b>1</b>
<b>MGU-SLIM3</b>	0,0817	0,1024	0,7738	-2627,20	-2445,44	0,0122	1,95E-05	-2622,88	42,08	0,0566	2
<b>GRU</b>	0,0830	0,1039	0,7970	-2400,06	-1683,90	0,0226	2,82E-05	-2398,57	40,06	0,3815	15
<b>GRU-SLIM1</b>	0,0823	0,1030	0,7820	-2579,70	-2435,88	0,0122	2E-05	-2574,98	40,96	0,1085	6
<b>GRU-SLIM2</b>	0,0826	0,1035	0,7907	-2647,31	-2564,15	0,0118	1,94E-05	-2642,32	41,07	0,0693	3
<b>GRU-SLIM3</b>	0,0819	0,1026	0,7759	-2565,52	-2232,18	0,0150	2,19E-05	-2562,48	42,25	0,1294	9
<b>LSTM-Vanilla</b>	0,0834	0,1046	0,8042	-2311,82	-1517,30	0,0312	3,66E-05	-2311,27	42,63	0,5036	18
<b>LSTM-SLIM1</b>	0,0826	0,1035	0,7890	-2252,23	-1304,66	0,0270	3,25E-05	-2254,49	41,19	0,4992	17
<b>LSTM-SLIM2</b>	0,0823	0,1032	0,7847	-2241,02	-1373,81	0,0260	3,17E-05	-2242,06	42,81	0,4575	16
<b>LSTM-SLIM3</b>	0,0816	0,1023	0,7719	-2535,86	-2287,80	0,0129	2,04E-05	-2532,17	42,25	0,1125	7

Table 21: Test results of RNN variants for time series data with Chaotic behavior.

	MAE	RMSE	TU	AIC	BIC	APC	HSP	SBIC	POCID	MCIM	Rank
<b>ELMAN</b>	0,0611	0,0768	2,8365	-3555,56	-3445,75	0,0105	1,66E-05	-3553,07	56,78	0,3312	13
<b>JORDAN</b>	0,0614	0,0776	0,8107	-3542,07	-3449,85	0,0102	1,67E-05	-3540,03	55,82	0,3344	14
<b>MRNN</b>	0,0606	0,0767	1,4364	-3449,87	-3293,96	0,0112	1,70E-05	-3449,98	55,98	0,3963	16
<b>IRNN</b>	0,0680	0,0842	0,6610	-3477,67	-3112,90	0,0161	2,37E-05	-3484,68	54,71	0,5457	20
<b>SCRN</b>	0,0556	0,0699	0,6424	-3637,80	-3422,59	0,0094	1,45E-05	-3639,88	55,80	0,1798	5
<b>MUT1</b>	0,0576	0,0726	0,5842	-3693,89	-3584,17	0,0093	1,51E-05	-3694,28	56,45	0,1521	2
<b>MUT2</b>	0,0609	0,0760	0,5364	-3514,34	-2980,48	0,0160	2,17E-05	-3527,04	57,72	0,3474	15
<b>MUT3</b>	0,0533	0,0671	0,5245	-3513,64	-2833,53	0,0187	2,21E-05	-3540,32	57,19	0,2659	6
<b>MGU</b>	0,0539	0,0679	0,5391	-3602,20	-3153,47	0,0117	1,62E-05	-3607,21	57,16	0,1701	3
<b>MGU-SLIM1</b>	0,0606	0,0757	0,5782	-3613,21	-3341,08	0,0122	1,83E-05	-3620,21	56,19	0,2794	8
<b>MGU-SLIM2</b>	0,0540	0,0679	0,5748	-3560,06	-3021,49	0,0105	1,52E-05	-3579,54	58,07	0,1729	4
<b>MGU-SLIM3</b>	0,0600	0,0752	7,0372	-3529,90	-3120,72	0,0143	2,07E-05	-3541,90	55,87	0,4650	18
<b>GRU</b>	0,0536	0,0676	0,4793	-3406,40	-2458,13	0,0189	2,25E-05	-3433,64	59,22	0,3104	11
<b>GRU-SLIM1</b>	0,0603	0,0753	0,5461	-3549,65	-3086,89	0,0122	1,83E-05	-3570,81	56,66	0,3129	12
<b>GRU-SLIM2</b>	0,0587	0,0740	0,5543	-3519,91	-2989,82	0,0115	1,73E-05	-3545,10	57,80	0,2836	9
<b>GRU-SLIM3</b>	0,0602	0,0752	0,5664	-3593,38	-3290,79	0,0127	1,87E-05	-3602,37	56,40	0,2851	10
<b>LSTM-Vanilla</b>	0,0532	0,0671	0,4772	-3475,04	-2677,35	0,0506	4,94E-05	-3486,80	59,06	0,4290	17
<b>LSTM-SLIM1</b>	0,0527	0,0664	0,4974	-3434,01	-2545,32	0,0122	1,65E-05	-3476,53	57,73	0,2696	7
<b>LSTM-SLIM2</b>	0,0533	0,0674	0,5045	-3290,49	-2110,00	0,0320	3,36E-05	-3330,35	58,74	0,4784	19
<b>LSTM-SLIM3</b>	<b>0,0532</b>	<b>0,0670</b>	<b>0,4927</b>	<b>-3701,04</b>	<b>-3370,02</b>	<b>0,0102</b>	<b>1,49E-05</b>	<b>-3708,28</b>	<b>57,05</b>	<b>0,0804</b>	<b>1</b>

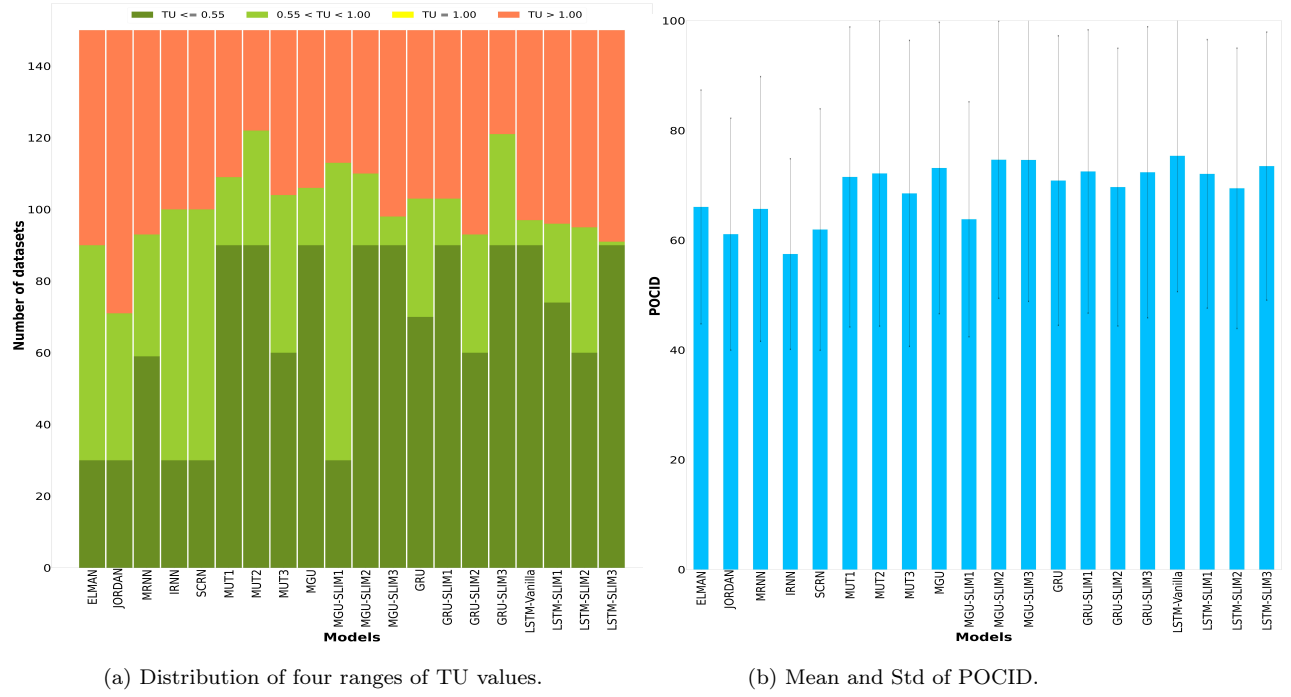


Figure 21: TU and POCID test results obtained by RNN cell structures on deterministic time series.

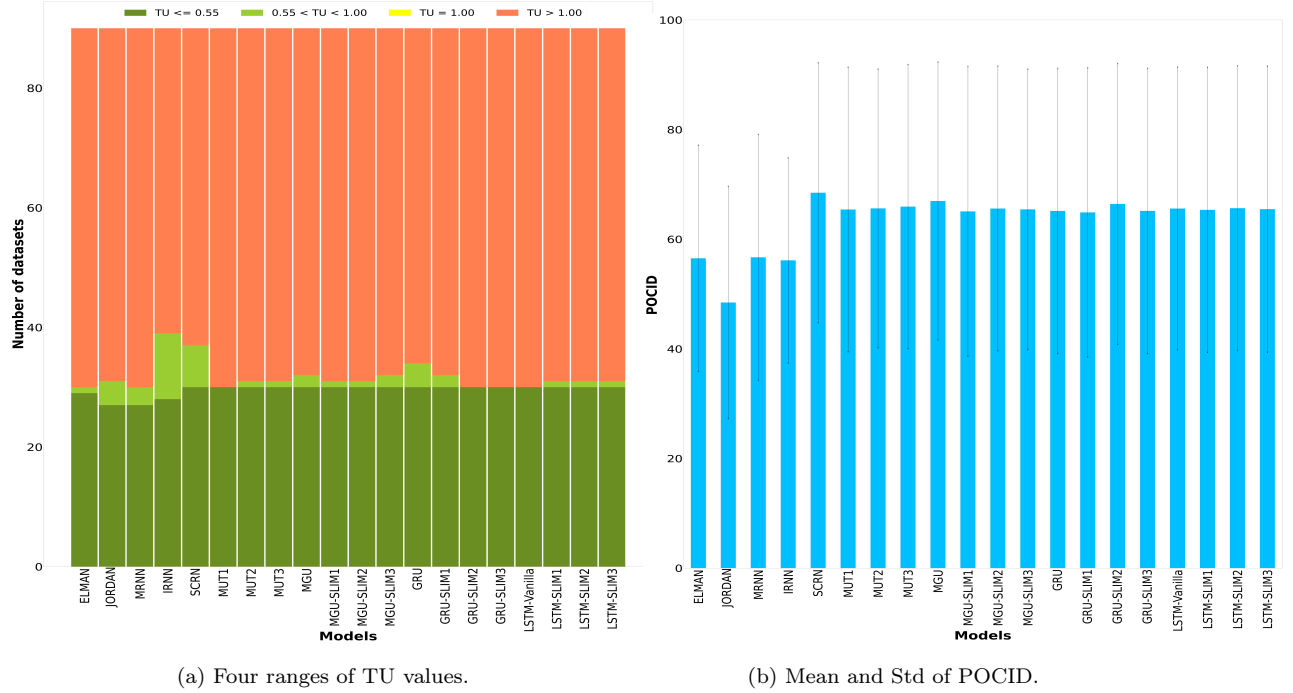


Figure 22: TU and POCID test results obtained by RNN cell structures on random-walk time series

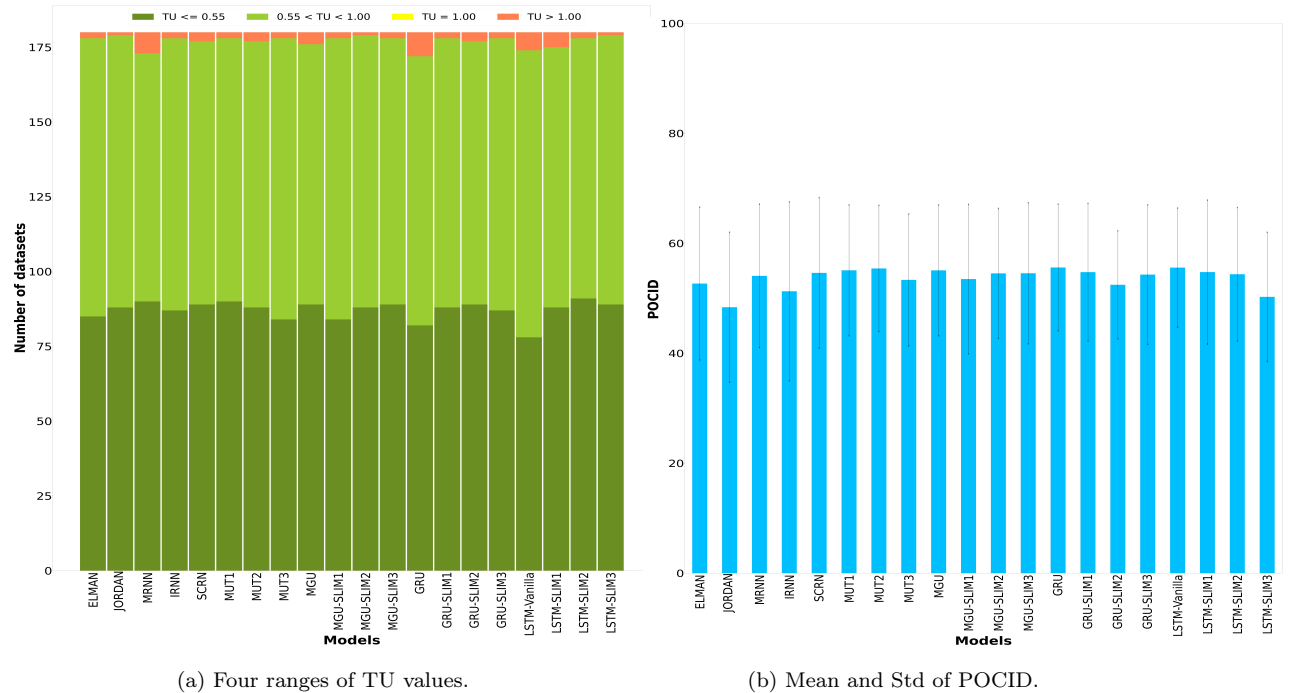


Figure 23: TU and POCID test results obtained by RNN cell structures on nonlinear time series

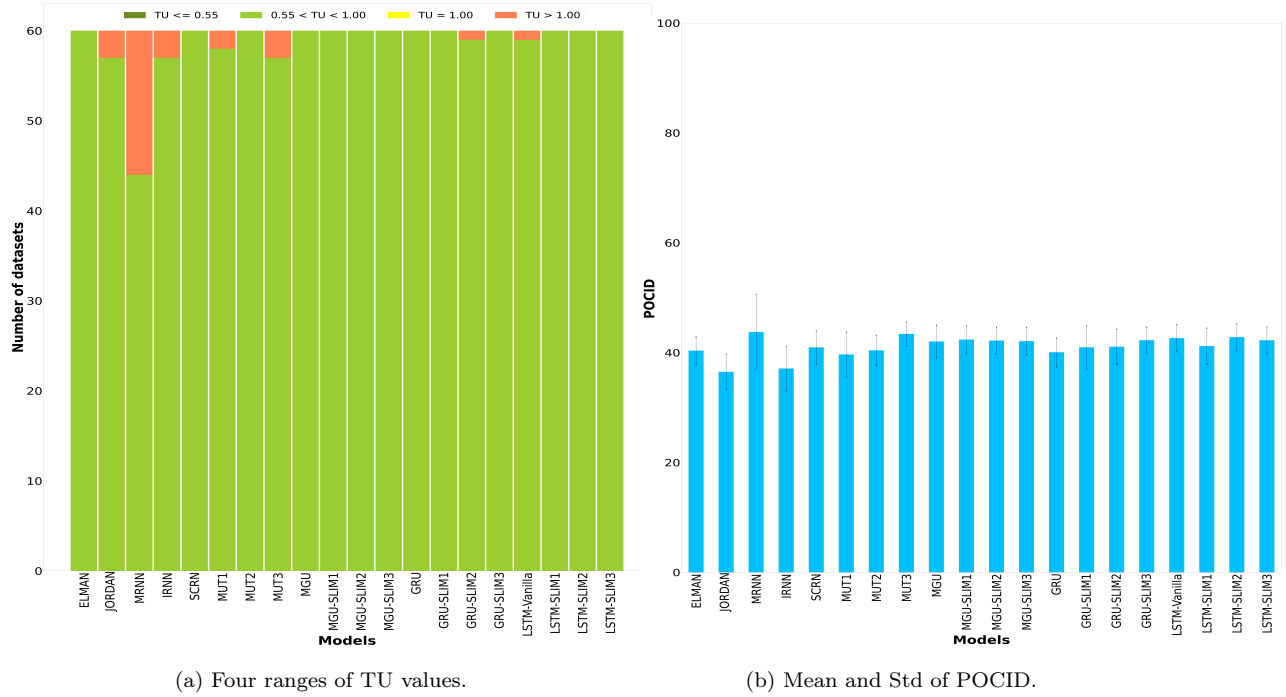


Figure 24: TU and POCID test results obtained by RNN cell structures on long-memory time series

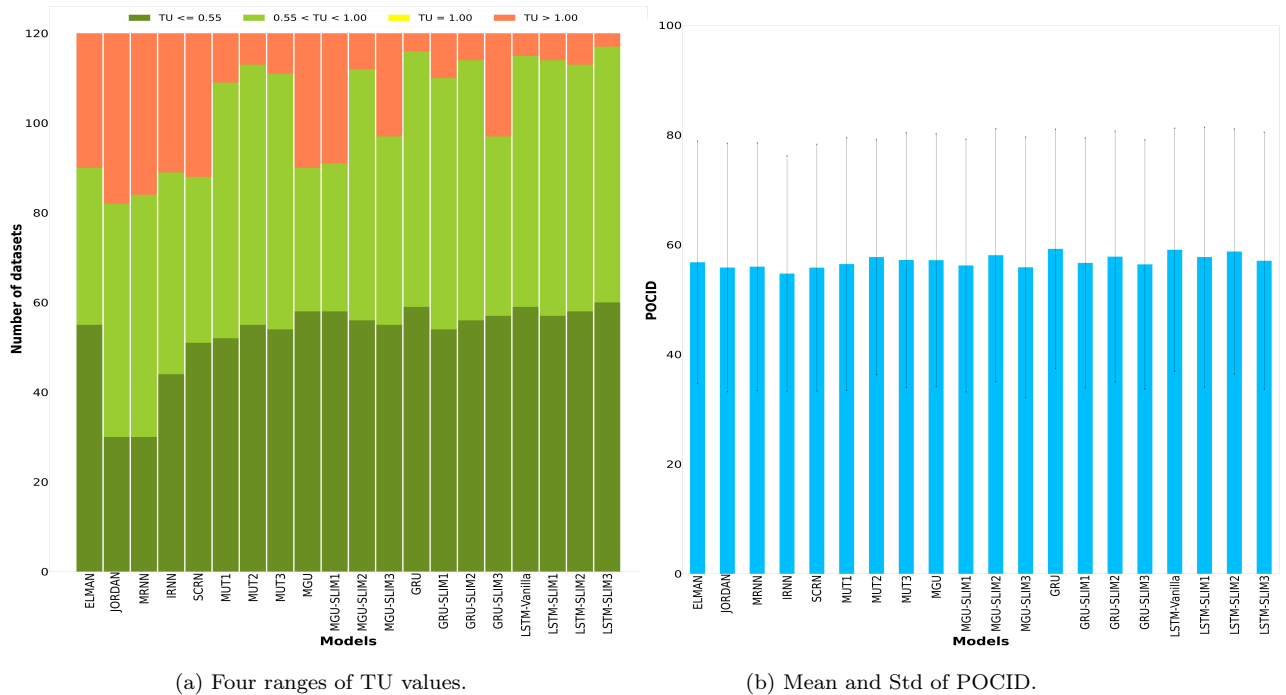
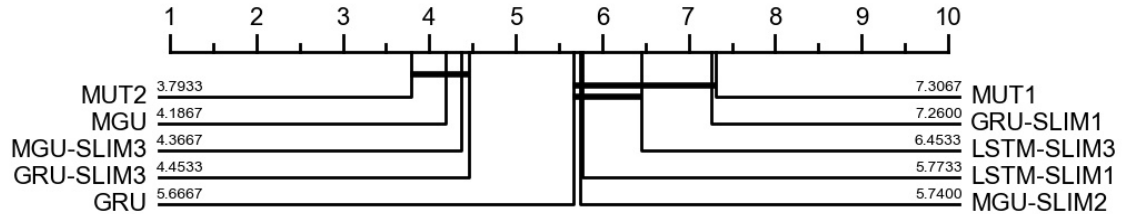
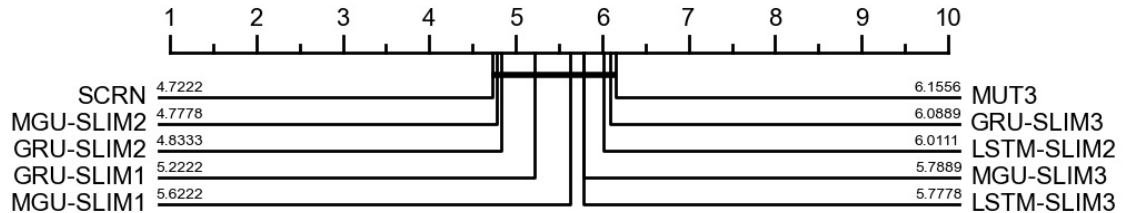


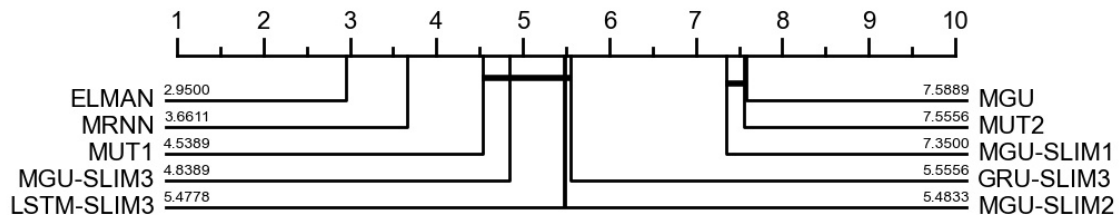
Figure 25: TU and POCID test results obtained by RNN cell structures on chaotic time series



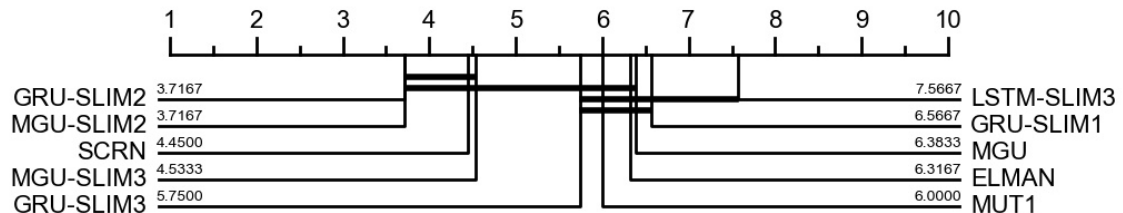
(a) Deterministic behavior.



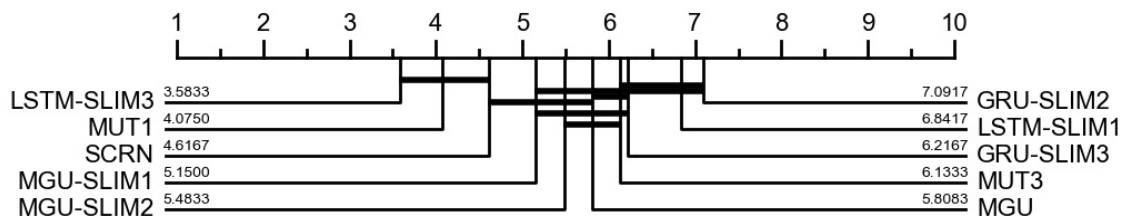
(b) Random-walk behavior.



(c) Nonlinear behavior.



(d) Long-memory behavior.



(e) Chaotic behavior.

Figure 26: CD diagrams for the MCIM values comparing the top 10 RNN cell structures on the five time series behaviors.

The results of the two experiments are summarized in Table 22. The MUT2, the SCRN, and the ELMAN models are the most recommended RNNs to forecast time series data with deterministic, random-walk, and nonlinear behaviors, respectively. Whereas, the MGU-SLIM2 and the LSTM-SLIM3 are the most recommended for the long-memory and chaotic behaviors, respectively.

Table 22: Summary of the test results for the two experiments.

Behaviors	Experiment 1		Experiment 2		Recommended cell
	Best cell	MCIM	Best cell	MCIM	
Deterministic	CIFG	0,1210	MUT2	0,0276	MUT2
Random-walk	CIFG	0,0830	SCRN	0,0361	SCRN
Nonlinear	NOG	0,2187	ELMAN	0,1635	ELMAN
Long-memory	NIG	0,0851	MGU-SLIM2	0,0438	MGU-SLIM2
Chaotic	NOG	0,2355	LSTM-SLIM3	0,0804	LSTM-SLIM3

## 7. Conclusions

In this paper, we proposed a comprehensive taxonomy of all possible time series behaviors, which are: deterministic, random-walk, nonlinear, long-memory, and chaotic. Then, we conducted two experiments to show the best RNN cell structure for each behavior. In the first experiment, we evaluated the LSTM-Vanilla model and 11 of its variants created based on one alteration in its basic architecture that consists in (1) removing (NIG, NFG, NOG, NIAF, NFAF, NOAF, and NCAF), (2) adding (PC and FGR), or (3) substituting (FB1 and CIFG) one cell component. While, in the second experiment, we evaluated LSTM-Vanilla along with a set of 19 RNN models based on other recurrent cell structures (JORDAN, ELMAN, MRNN, SCRN, IRNN, GRU, MGU, MUT1, MUT2, MUT3, and 9 SLIM variants).

To evaluate, compare, and select the best model, different statistical metrics were used: error-based metrics (MAE and RMSE), information criterion-based metrics (AIC, BIC, APC, HSP, and SBIC), naïve-based metric (TU), and direction change-based metric (POCID). To facilitate the task of the best model selection, a new statistical metric was proposed (MCIM). Further to improve our confidence in the models' interpretation and selection, Friedman Wilcoxon-Holm signed-rank test was used.

In the first experiment, We showed that the CIFG model is the most suitable for non-stationary time series due to the existence of deterministic behavior or random-walk behavior. We also, experimentally, proved that the NOG model is the most performing for the nonlinear and chaotic behaviors, while the NIG model outperformed the other models with respect to long-memory behavior. In the second experiment, over the 20 evaluated RNN models, the best forecasting results were achieved by the new parameter-reduced variants of MGU (MGU-SLIM2) and LSTM (LSTM-SLIM3) for the long-memory and chaotic behaviors, respectively. For the deterministic behavior, the best significant model is MUT2. In the case of the random-walk behavior, the most significantly better model is SCRN. Finally, for the nonlinear behavior, the ELMAN

model is the best significant model.

Based on the outcomes of both experiments, we arrived to demonstrate that the SLIM3 version of the LSTM cell has the highest ability to increase the performance of the RNN model in forecasting chaotic behavior. While the SLIM2 version of the MGU model is recommended in the case of time series with long-memory behavior. Finally, the MUT2, SCRN, and ELMAN variants are the strongly advocated models to forecast time series data with deterministic, random-walk, and nonlinear behaviors, respectively. The outcomes of our study are limited to time series with a single behavior. However, in real-world problems, combined behaviors (i.e., more than one behavior in the same time series) can also occur. In future work, evaluating the best RNN cell with respect to such types of time series can complement the guidelines provided by this study.

## Acknowledgements

This work was partially supported by DETECTOR (A-RNM-256-UGR18 Universidad de Granada/FEDER), LifeWatch SmartEcomountains (LifeWatch-2019-10-UGR-01 Ministerio de Ciencia e Innovación/Universidad de Granada/FEDER), DeepL-ISCO (A-TIC-458-UGR18 Ministerio de Ciencia e Innovación/FEDER), BigDDL-CET (P18-FR-4961 Ministerio de Ciencia e Innovación/Universidad de Granada/FEDER).

## References

- Abdulkarim, S. (2016). Time series prediction with simple recurrent neural networks. *Bayero Journal of Pure and Applied Sciences*, 9, 19–24.
- Akaike, H. (1969). Fitting autoregressive models for prediction. *Annals of the institute of Statistical Mathematics*, 21, 243–247.
- Alkhayat, G., & Mehmood, R. (2021). A review and taxonomy of wind and solar energy forecasting methods based on deep learning. *Energy and AI*, (p. 100060).
- Amemiya, T. (1980). Selection of regressors. *International economic review*, (pp. 331–354).
- Athiyarath, S., Paul, M., & Krishnaswamy, S. (2020). A comparative study and analysis of time series forecasting techniques. *SN Computer Science*, 1, 1–7.
- Benavoli, A., Corani, G., & Mangili, F. (2016). Should we really use post-hoc tests based on mean-ranks? *The Journal of Machine Learning Research*, 17, 152–161.
- Bensaïda, A., & Litimi, H. (2013). High level chaos in the exchange and index markets. *Chaos, Solitons & Fractals*, 54, 90–95.

- Bianchi, F. M., Maiorino, E., Kampffmeyer, M. C., Rizzi, A., & Jenssen, R. (2017). An overview and comparative analysis of recurrent neural networks for short term load forecasting. *arXiv preprint arXiv:1705.04378*, .
- Boaretto, B., Budzinski, R. C., Rossi, K. L., Prado, T. L., Lopes, S. R., & Masoller, C. (2021). Discriminating chaotic and stochastic time series using permutation entropy and artificial neural networks. *Scientific reports*, 11, 1–10.
- Bourdeau, M., qiang Zhai, X., Nefzaoui, E., Guo, X., & Chatellier, P. (2019). Modeling and forecasting building energy consumption: A review of data-driven techniques. *Sustainable Cities and Society*, 48, 101533.
- Box, G. E., Jenkins, G. M., Reinsel, G. C., & Ljung, G. M. (2015). *Time series analysis: forecasting and control*. John Wiley & Sons.
- Bukhari, A. H., Raja, M. A. Z., Sulaiman, M., Islam, S., Shoaib, M., & Kumam, P. (2020). Fractional neuro-sequential arfima-lstm for financial market forecasting. *IEEE Access*, 8, 71326–71338.
- Cencini, M., Falcioni, M., Olbrich, E., Kantz, H., & Vulpiani, A. (2000). Chaos or noise: Difficulties of a distinction. *Physical Review E*, 62, 427.
- Chandra, R., & Zhang, M. (2012). Cooperative coevolution of elman recurrent neural networks for chaotic time series prediction. *Neurocomputing*, 86, 116–123.
- Chatfield, C. (2013). *The analysis of time series: theory and practice*. Springer.
- Chimmula, V. K. R., & Zhang, L. (2020). Time series forecasting of covid-19 transmission in canada using lstm networks. *Chaos, Solitons & Fractals*, 135, 109864.
- Cho, K., Van Merriënboer, B., Gulcehre, C., Bahdanau, D., Bougares, F., Schwenk, H., & Bengio, Y. (2014). Learning phrase representations using rnn encoder-decoder for statistical machine translation. *arXiv preprint arXiv:1406.1078*, .
- Choubin, B., Zehtabian, G., Azareh, A., Rafiei-Sardooi, E., Sajedi-Hosseini, F., & Kiş, Ö. (2018). Precipitation forecasting using classification and regression trees (cart) model: a comparative study of different approaches. *Environmental earth sciences*, 77, 1–13.
- Crone, S. (2008). Nn5 forecasting competition for artificial neural networks & computational intelligence.
- Dau, H. A., Bagnall, A., Kamgar, K., Yeh, C.-C. M., Zhu, Y., Gharghabi, S., Ratanamahatana, C. A., & Keogh, E. (2019). The ucr time series archive. *IEEE/CAA Journal of Automatica Sinica*, 6, 1293–1305.
- Demšar, J. (2006). Statistical comparisons of classifiers over multiple data sets. *The Journal of Machine learning research*, 7, 1–30.

- Dey, R., & Salem, F. M. (2017). Gate-variants of gated recurrent unit (gru) neural networks. In *2017 IEEE 60th international midwest symposium on circuits and systems (MWSCAS)* (pp. 1597–1600). IEEE.
- Dickey, D. A., & Fuller, W. A. (1979). Distribution of the estimators for autoregressive time series with a unit root. *Journal of the American statistical association*, *74*, 427–431.
- Divina, F., Garcia Torres, M., Goméz Vela, F. A., & Vazquez Noguera, J. L. (2019). A comparative study of time series forecasting methods for short term electric energy consumption prediction in smart buildings. *Energies*, *12*, 1934.
- Dudek, G. (2016). Neural networks for pattern-based short-term load forecasting: A comparative study. *Neurocomputing*, *205*, 64–74.
- Eckmann, J.-P., & Ruelle, D. (1985). Ergodic theory of chaos and strange attractors. *The theory of chaotic attractors*, (pp. 273–312).
- Elman, J. L. (1990). Finding structure in time. *Cognitive science*, *14*, 179–211.
- Erdelj, M., Król, M., & Natalizio, E. (2017). Wireless sensor networks and multi-uav systems for natural disaster management. *Computer Networks*, *124*, 72–86.
- Findley, D. F. (1991). Counterexamples to parsimony and bic. *Annals of the Institute of Statistical Mathematics*, *43*, 505–514.
- Fischer, T., Krauss, C., & Treichel, A. (2018). *Machine learning for time series forecasting-a simulation study*. Technical Report FAU Discussion Papers in Economics.
- Friedman, M. (1940). A comparison of alternative tests of significance for the problem of m rankings. *The Annals of Mathematical Statistics*, *11*, 86–92.
- Garcia, S., & Herrera, F. (2008). An extension on " statistical comparisons of classifiers over multiple data sets" for all pairwise comparisons. *Journal of machine learning research*, *9*.
- Gers, F. A., & Schmidhuber, E. (2001). Lstm recurrent networks learn simple context-free and context-sensitive languages. *IEEE Transactions on Neural Networks*, *12*, 1333–1340.
- Gers, F. A., & Schmidhuber, J. (2000). Recurrent nets that time and count. In *Proceedings of the IEEE-INNS-ENNS International Joint Conference on Neural Networks. IJCNN 2000. Neural Computing: New Challenges and Perspectives for the New Millennium* (pp. 189–194). IEEE volume 3.
- Gers, F. A., Schmidhuber, J., & Cummins, F. (2000). Learning to forget: Continual prediction with lstm. *Neural computation*, *12*, 2451–2471.
- Gers, F. A., Schraudolph, N. N., & Schmidhuber, J. (2002). Learning precise timing with lstm recurrent networks. *Journal of machine learning research*, *3*, 115–143.

- Geweke, J., & Porter-Hudak, S. (1983). The estimation and application of long memory time series models. *Journal of time series analysis*, 4, 221–238.
- Giuliari, F., Hasan, I., Cristani, M., & Galasso, F. (2021). Transformer networks for trajectory forecasting. In *2020 25th International Conference on Pattern Recognition (ICPR)* (pp. 10335–10342). IEEE.
- Godahewa, R., Bergmeir, C., & Webb, G. (2020). Cif 2016 dataset. URL: <https://doi.org/10.5281/zenodo.3904073>. doi:10.5281/zenodo.3904073.
- Godahewa, R., Bergmeir, C., Webb, G. I., Hyndman, R. J., & Montero-Manso, P. (2021). Monash time series forecasting archive. *arXiv preprint arXiv:2105.06643*, .
- Gottwald, G. A., & Melbourne, I. (2004). A new test for chaos in deterministic systems. *Proceedings of the Royal Society of London. Series A: Mathematical, Physical and Engineering Sciences*, 460, 603–611.
- Granata, F. (2019). Evapotranspiration evaluation models based on machine learning algorithms—a comparative study. *Agricultural Water Management*, 217, 303–315.
- Grassberger, P., & Procaccia, I. (1984). Dimensions and entropies of strange attractors from a fluctuating dynamics approach. *Physica D: Nonlinear Phenomena*, 13, 34–54.
- Grau-Carles, P. (2005). Tests of long memory: A bootstrap approach. *Computational Economics*, 25, 103–113.
- Graves, A., Wayne, G., & Danihelka, I. (2014). Neural turing machines. *arXiv preprint arXiv:1410.5401*, .
- Greff, K., Srivastava, R. K., Koutník, J., Steunebrink, B. R., & Schmidhuber, J. (2016). Lstm: A search space odyssey. *IEEE transactions on neural networks and learning systems*, 28, 2222–2232.
- He, K., Zhang, X., Ren, S., & Sun, J. (2015). Delving deep into rectifiers: Surpassing human-level performance on imagenet classification. In *Proceedings of the IEEE international conference on computer vision* (pp. 1026–1034).
- Heck, J. C., & Salem, F. M. (2017). Simplified minimal gated unit variations for recurrent neural networks. In *2017 IEEE 60th International Midwest Symposium on Circuits and Systems (MWSCAS)* (pp. 1593–1596). IEEE.
- Hochreiter, S., & Schmidhuber, J. (1997). Long short-term memory. *Neural computation*, 9, 1735–1780.
- Hocking, R. R. (1976). A biometrics invited paper. the analysis and selection of variables in linear regression. *Biometrics*, (pp. 1–49).
- Holm, S. (1979). A simple sequentially rejective multiple test procedure. *Scandinavian journal of statistics*, (pp. 65–70).

- Ingla-Perez, L. (2020). A comprehensive framework for uncovering non-linearity and chaos in financial markets: Empirical evidence for four major stock market indices. *Entropy*, 22, 1435.
- Irie, K., Tüske, Z., Alkhouri, T., Schlüter, R., Ney, H. et al. (2016). Lstm, gru, highway and a bit of attention: an empirical overview for language modeling in speech recognition. In *Interspeech* (pp. 3519–3523).
- Jing, L., Gulcehre, C., Peurifoy, J., Shen, Y., Tegmark, M., Soljacic, M., & Bengio, Y. (2019). Gated orthogonal recurrent units: On learning to forget. *Neural computation*, 31, 765–783.
- Jordan, M. (1989). Serial order: A parallel distributed processing approach advances in connectionist theory.
- Jozefowicz, R., Zaremba, W., & Sutskever, I. (2015). An empirical exploration of recurrent network architectures. In *International conference on machine learning* (pp. 2342–2350). PMLR.
- Kang, Y., Hyndman, R. J., & Li, F. (2020). Gratis: Generating time series with diverse and controllable characteristics. *Statistical Analysis and Data Mining: The ASA Data Science Journal*, 13, 354–376.
- Kaplan, D. T. (1994). Exceptional events as evidence for determinism. *Physica D: Nonlinear Phenomena*, 73, 38–48.
- Keenan, D. M. (1985). A tukey nonadditivity-type test for time series nonlinearity. *Biometrika*, 72, 39–44.
- Keogh, E., & Kasetty, S. (2003). On the need for time series data mining benchmarks: a survey and empirical demonstration. *Data Mining and knowledge discovery*, 7, 349–371.
- Khaldi, R., El Afia, A., & Chiheb, R. (2019a). Forecasting of btc volatility: comparative study between parametric and nonparametric models. *Progress in Artificial Intelligence*, 8, 511–523.
- Khaldi, R., El Afia, A., & Chiheb, R. (2019b). Forecasting of weekly patient visits to emergency department: real case study. *Procedia computer science*, 148, 532–541.
- Kim, J.-M., & Jung, H. (2018). Time series forecasting using functional partial least square regression with stochastic volatility, garch, and exponential smoothing. *Journal of Forecasting*, 37, 269–280.
- Kingma, D. P., & Ba, J. (2014). Adam: A method for stochastic optimization. *arXiv preprint arXiv:1412.6980*, .
- Kwiatkowski, D., Phillips, P. C., Schmidt, P., & Shin, Y. (1992). Testing the null hypothesis of stationarity against the alternative of a unit root: How sure are we that economic time series have a unit root? *Journal of econometrics*, 54, 159–178.
- Le, Q. V., Jaitly, N., & Hinton, G. E. (2015). A simple way to initialize recurrent networks of rectified linear units. *arXiv preprint arXiv:1504.00941*, .

- Li, Q., & Lin, R.-C. (2016). A new approach for chaotic time series prediction using recurrent neural network. *Mathematical Problems in Engineering*, 2016.
- Lim, T. P., & Puthusserypady, S. (2007). Chaotic time series prediction and additive white gaussian noise. *Physics letters A*, 365, 309–314.
- Liu, H., Yan, G., Duan, Z., & Chen, C. (2021). Intelligent modeling strategies for forecasting air quality time series: A review. *Applied Soft Computing*, (p. 106957).
- Liu, K., Chen, Y., & Zhang, X. (2017). An evaluation of arfima (autoregressive fractional integral moving average) programs. *Axioms*, 6, 16.
- Liu, S., Ji, H., & Wang, M. C. (2019). Nonpooling convolutional neural network forecasting for seasonal time series with trends. *IEEE transactions on neural networks and learning systems*, 31, 2879–2888.
- Liu, Y. (2019). Novel volatility forecasting using deep learning–long short term memory recurrent neural networks. *Expert Systems with Applications*, 132, 99–109.
- Lo, A. W. (1991). Long-term memory in stock market prices. *Econometrica: Journal of the Econometric Society*, (pp. 1279–1313).
- López-Caraballo, C., Salfate, I., Lazzús, J., Rojas, P., Rivera, M., & Palma-Chilla, L. (2016). Mackey-glass noisy chaotic time series prediction by a swarm-optimized neural network. In *Journal of Physics: Conference Series* (p. 012002). IOP Publishing volume 720.
- Lu, Y., & Salem, F. M. (2017). Simplified gating in long short-term memory (lstm) recurrent neural networks. In *2017 IEEE 60th International Midwest Symposium on Circuits and Systems (MWSCAS)* (pp. 1601–1604). IEEE.
- Ma, Q.-L., Zheng, Q.-L., Peng, H., Zhong, T.-W., & Xu, L.-Q. (2007). Chaotic time series prediction based on evolving recurrent neural networks. In *2007 international conference on machine learning and cybernetics* (pp. 3496–3500). IEEE volume 6.
- Maeng, K., Kim, J., & Shin, J. (2020). Demand forecasting for the 5g service market considering consumer preference and purchase delay behavior. *Telematics and Informatics*, 47, 101327.
- Makridakis, S., Spiliotis, E., & Assimakopoulos, V. (2018). The m4 competition: Results, findings, conclusion and way forward. *International Journal of Forecasting*, 34, 802–808.
- Mandelbrot, B. B., & Wallis, J. R. (1968). Noah, joseph, and operational hydrology. *Water resources research*, 4, 909–918.
- Matilla-García, M., & Marín, M. R. (2010). A new test for chaos and determinism based on symbolic dynamics. *Journal of Economic Behavior & Organization*, 76, 600–614.

- Mikolov, T., Joulin, A., Chopra, S., Mathieu, M., & Ranzato, M. (2014). Learning longer memory in recurrent neural networks. *arXiv preprint arXiv:1412.7753*, .
- Montgomery, D. C., Jennings, C. L., & Kulahci, M. (2015). *Introduction to time series analysis and forecasting*. John Wiley & Sons.
- Murat, M., Malinowska, I., Gos, M., & Krzyszczak, J. (2018). Forecasting daily meteorological time series using arima and regression models. *International agrophysics*, 32.
- Neil, D., Pfeiffer, M., & Liu, S.-C. (2016). Phased lstm: Accelerating recurrent network training for long or event-based sequences. *arXiv preprint arXiv:1610.09513*, .
- Nina, O., & Rodriguez, A. (2015). Simplified lstm unit and search space probability exploration for image description. In *2015 10th International Conference on Information, Communications and Signal Processing (ICICS)* (pp. 1–5). IEEE.
- Olson, R. S., La Cava, W., Orzechowski, P., Urbanowicz, R. J., & Moore, J. H. (2017). Pmlb: a large benchmark suite for machine learning evaluation and comparison. *BioData mining*, 10, 1–13.
- Palma, W. (2007). *Long-memory time series: theory and methods* volume 662. John Wiley & Sons.
- Papacharalampous, G., & Tyralis, H. (2020). Hydrological time series forecasting using simple combinations: Big data testing and investigations on one-year ahead river flow predictability. *Journal of Hydrology*, 590, 125205.
- Parmezan, A. R. S., Souza, V. M., & Batista, G. E. (2019). Evaluation of statistical and machine learning models for time series prediction: Identifying the state-of-the-art and the best conditions for the use of each model. *Information sciences*, 484, 302–337.
- Pascanu, R., Mikolov, T., & Bengio, Y. (2013). On the difficulty of training recurrent neural networks. In *International conference on machine learning* (pp. 1310–1318). PMLR.
- Peng, C.-K., Buldyrev, S. V., Havlin, S., Simons, M., Stanley, H. E., & Goldberger, A. L. (1994). Mosaic organization of dna nucleotides. *Physical review e*, 49, 1685.
- Phillips, P. C., & Perron, P. (1988). Testing for a unit root in time series regression. *Biometrika*, 75, 335–346.
- Pulver, A., & Lyu, S. (2017). Lstm with working memory. In *2017 International Joint Conference on Neural Networks (IJCNN)* (pp. 845–851). IEEE.
- Qu, Z. (2011). A test against spurious long memory. *Journal of Business & Economic Statistics*, 29, 423–438.
- Rajagukguk, R. A., Ramadhan, R. A., & Lee, H.-J. (2020). A review on deep learning models for forecasting time series data of solar irradiance and photovoltaic power. *Energies*, 13, 6623.

- Ramakrishnan, N., & Soni, T. (2018). Network traffic prediction using recurrent neural networks. In *2018 17th IEEE International Conference on Machine Learning and Applications (ICMLA)* (pp. 187–193). IEEE.
- Runge, J., & Zmeureanu, R. (2021). A review of deep learning techniques for forecasting energy use in buildings. *Energies*, 14, 608.
- Sagheer, A., & Kotb, M. (2019). Time series forecasting of petroleum production using deep lstm recurrent networks. *Neurocomputing*, 323, 203–213.
- Salles, R., Belloze, K., Porto, F., Gonzalez, P. H., & Ogasawara, E. (2019). Nonstationary time series transformation methods: An experimental review. *Knowledge-Based Systems*, 164, 274–291.
- Sangiorgio, M., Dercole, F., & Guariso, G. (2021). Forecasting of noisy chaotic systems with deep neural networks. *Chaos, Solitons & Fractals*, 153, 111570.
- Sawa, T. (1978). Information criteria for discriminating among alternative regression models. *Econometrica: Journal of the Econometric Society*, (pp. 1273–1291).
- Sezer, O. B., Gudelek, M. U., & Ozbayoglu, A. M. (2020). Financial time series forecasting with deep learning: A systematic literature review: 2005–2019. *Applied Soft Computing*, 90, 106181.
- Siami-Namini, S., & Namin, A. S. (2018). Forecasting economics and financial time series: Arima vs. lstm. *arXiv preprint arXiv:1803.06386*, .
- Spiliotis, E., Kouloumos, A., Assimakopoulos, V., & Makridakis, S. (2020). Are forecasting competitions data representative of the reality? *International Journal of Forecasting*, 36, 37–53.
- Sutskever, I., Vinyals, O., & Le, Q. V. (2014). Sequence to sequence learning with neural networks. In *Advances in neural information processing systems* (pp. 3104–3112).
- Teräsvirta, T., Lin, C.-F., & Granger, C. W. (1993). Power of the neural network linearity test. *Journal of time series analysis*, 14, 209–220.
- Tian, Z. (2019). Chaotic characteristic analysis of short-term wind speed time series with different time scales. *Energy Sources, Part A: Recovery, Utilization, and Environmental Effects*, (pp. 1–15).
- Tsay, R. S. (1986). Nonlinearity tests for time series. *Biometrika*, 73, 461–466.
- Veeriah, V., Zhuang, N., & Qi, G.-J. (2015). Differential recurrent neural networks for action recognition. In *Proceedings of the IEEE international conference on computer vision* (pp. 4041–4049).
- Vinyals, O., Toshev, A., Bengio, S., & Erhan, D. (2015). Show and tell: A neural image caption generator. In *Proceedings of the IEEE conference on computer vision and pattern recognition* (pp. 3156–3164).

- Wales, D. J. (1991). Calculating the rate of loss of information from chaotic time series by forecasting. *Nature*, 350, 485–488.
- Wang, Y.-C., & Chen, T.-C. T. (2018). A direct-solution fuzzy collaborative intelligence approach for yield forecasting in semiconductor manufacturing. *Procedia Manufacturing*, 17, 110–117.
- Wang, Z., Fathollahzadeh Attar, N., Khalili, K., Behmanesh, J., Band, S. S., Mosavi, A., & Chau, K.-w. (2020). Monthly streamflow prediction using a hybrid stochastic-deterministic approach for parsimonious non-linear time series modeling. *Engineering Applications of Computational Fluid Mechanics*, 14, 1351–1372.
- Werbos, P. J. (1990). Backpropagation through time: what it does and how to do it. *Proceedings of the IEEE*, 78, 1550–1560.
- Weston, J., Chopra, S., & Bordes, A. (2014). Memory networks. *arXiv preprint arXiv:1410.3916*, .
- White, H. (1989). An additional hidden unit test for neglected nonlinearity in multilayer feedforward networks. In *Proceedings of the international joint conference on neural networks* (pp. 451–455). Washington, DC volume 2.
- Wilcoxon, F. (1992). Individual comparisons by ranking methods. In *Breakthroughs in statistics* (pp. 196–202). Springer.
- Yamak, P. T., Yujian, L., & Gadosey, P. K. (2019). A comparison between arima, lstm, and gru for time series forecasting. In *Proceedings of the 2019 2nd International Conference on Algorithms, Computing and Artificial Intelligence* (pp. 49–55).
- Yeo, K. (2017). Model-free prediction of noisy chaotic time series by deep learning. *arXiv preprint arXiv:1710.01693*, .
- Yu, H., Ming, L. J., Sumei, R., & Shuping, Z. (2020). A hybrid model for financial time series forecasting—integration of ewt, arima with the improved abc optimized elm. *IEEE Access*, 8, 84501–84518.
- Zhang, G. P., Patuwo, B. E., & Hu, M. Y. (2001). A simulation study of artificial neural networks for nonlinear time-series forecasting. *Computers & Operations Research*, 28, 381–396.
- Zhang, G. P., & Qi, M. (2005). Neural network forecasting for seasonal and trend time series. *European journal of operational research*, 160, 501–514.
- Zhou, G.-B., Wu, J., Zhang, C.-L., & Zhou, Z.-H. (2016). Minimal gated unit for recurrent neural networks. *International Journal of Automation and Computing*, 13, 226–234.
- Zunino, L., Soriano, M. C., & Rosso, O. A. (2012). Distinguishing chaotic and stochastic dynamics from time series by using a multiscale symbolic approach. *Physical Review E*, 86, 046210.

## Appendix A. Architectures of the studied RNN cells

In this section, we provide the cell structures of the different RNN models along with their cellular calculations. To understand the calculations, Table A.23 presents the deception of the mathematical notations. To better understand the components inside the LSTM-Vanilla cell, we present below the role of the main elements:

- Input state  $x_t$ : it contains the data features at time step  $t$ .
- Output state  $y_t$ : it contains the output of the model at time step  $t$ .
- Hidden state  $h_t$ : it represents the short-term memory of the cell at time step  $t$ .
- Cell state  $c_t$ : it represents the long-term memory of the cell at time step  $t$ .
- Candidate cell state  $\tilde{c}_t$ : it contains the new information we can use to update the cell state at time step  $t$ .
- Input gate  $\Gamma_{i_t}$ : it filters from the current candidate cell state the information that should be used to update the current cell state.
- Forget gate  $\Gamma_{f_t}$ : it filters from the previous cell state the information that should be used to update the current cell state.
- Output gate  $\Gamma_{o_t}$ : it filters from the current cell state the information that should be exposed to the external network (the next time step and the next hidden and/or output layer).

Table A.23: Nomenclature

Symbol	Significance
$x_t$	the input state at time step $t$ .
$h_t$	the hidden state at time step $t$ .
$y_t$	the output state at time step $t$ .
$\Gamma_{i_t}$	the input gate at time step $t$ .
$\Gamma_{f_t}$	the forget gate at time step $t$ .
$\Gamma_{o_t}$	the output gate at time step $t$ .
$\Gamma_{u_t}$	the update gate at time step $t$ .
$\Gamma_{r_t}$	the relevance gate at time step $t$ .
$c_t$	the cell state at time step $t$ .
$\tilde{c}_t$	the candidate cell state at time step $t$ .
$W_{xh}$	the weight matrix between the input and the hidden states.
$W_{hh}$	the weight matrix between the previous and the current hidden states.

Table A.23: Nomenclature

Symbol	Significance
$W_{hy}$	the weight matrix between the hidden and the output states.
$W_{yh}$	the weight matrix between the output and the hidden states.
$W_{xs}$	the weight matrix between the input and the context states.
$W_{sh}$	the weight matrix between the context and the hidden states.
$W_{sy}$	the weight matrix between the context and the output states.
$W_{xi}$	the weight matrix between the input state and the input gate.
$W_{hi}$	the weight matrix between the hidden state and the input gate.
$W_{xo}$	the weight matrix between the input state and the output gate.
$W_{ho}$	the weight matrix between the hidden state and the output gate.
$W_{xf}$	the weight matrix between the input state and the forget gate.
$W_{hf}$	the weight matrix between the hidden state and the forget gate.
$W_{x\tilde{c}}$	the weight matrix between the input state and the candidate cell state.
$W_{h\tilde{c}}$	the weight matrix between the hidden state and the candidate cell state.
$W_{x\tilde{h}}$	the weight matrix between the input state and the candidate hidden state.
$W_{h\tilde{h}}$	the weight matrix between the hidden state and the candidate hidden state.
$W_{ci}$	the weight matrix between the cell state and the input gate.
$W_{cf}$	the weight matrix between the cell state and the forget gate.
$W_{co}$	the weight matrix between the cell state and the output gate.
$W_{xu}$	the weight matrix between the input state and the update gate.
$W_{hu}$	the weight matrix between the hidden state and the update gate.
$W_{xr}$	the weight matrix between the input state and the relevance gate.
$W_{hr}$	the weight matrix between the hidden state and the relevance gate.
$W_{ii}$	the weight matrix between the previous and the current input gates.
$W_{ff}$	the weight matrix between the previous and the current forget gates.
$W_{oo}$	the weight matrix between the previous and the current output gates.
$W_{if}$	the weight matrix between the previous input gate and the current forget gate.
$W_{io}$	the weight matrix between the previous input gate and the current output gate.
$W_{fi}$	the weight matrix between the previous forget gate and the current input gate.
$W_{fo}$	the weight matrix between the previous forget gate and the current output gate.
$W_{oi}$	the weight matrix between the previous output gate and the current input gate.
$W_{of}$	the weight matrix between the previous output gate and the current forget gate.
$b_h$	the bias related to the hidden state.
$b_y$	the bias related to the output state.
$b_{\tilde{c}}$	the bias related to the candidate cell state.

Table A.23: Nomenclature

Symbol	Significance
$b_{\tilde{h}}$	the bias related to the candidate hidden state.
$b_i$	the bias related to the input gate.
$b_o$	the bias related to the output gate.
$b_f$	the bias related to the forget gate.
$b_u$	the bias related to the update gate.
$b_r$	the bias related to the relevance gate.
$g$	the activation function of the output state (the identity function).
$\otimes$	the point-wise multiplication (Hadamard product) presented in the figures as $\odot$ .
$\sigma$	the sigmoid activation function.

Table A.24: Description of different LSTM-Vanilla cell structures created based on one change in its architecture.

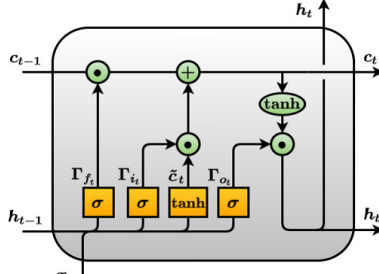
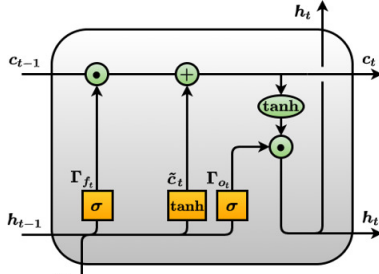
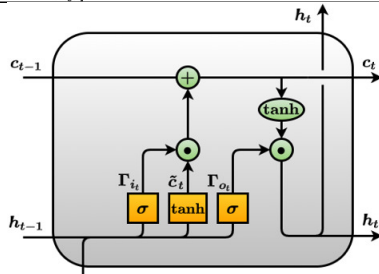
Cell name	Cell architecture	Cell computations
LSTM-Vanilla		$\tilde{c}_t = \tanh(x_t \cdot W_{x\tilde{c}} + h_{t-1} \cdot W_{h\tilde{c}} + b_{\tilde{c}})$ $\Gamma_{i_t} = \sigma(x_t \cdot W_{xi} + h_{t-1} \cdot W_{hi} + b_i)$ $\Gamma_{f_t} = \sigma(x_t \cdot W_{xf} + h_{t-1} \cdot W_{hf} + b_f)$ $\Gamma_{o_t} = \sigma(x_t \cdot W_{xo} + h_{t-1} \cdot W_{ho} + b_o)$ $c_t = \Gamma_{f_t} \otimes c_{t-1} + \Gamma_{i_t} \otimes \tilde{c}_t$ $h_t = \Gamma_{o_t} \otimes \tanh(c_t)$
LSTM-NIG		$\tilde{c}_t = \tanh(x_t \cdot W_{x\tilde{c}} + h_{t-1} \cdot W_{h\tilde{c}} + b_{\tilde{c}})$ $\Gamma_{f_t} = \sigma(x_t \cdot W_{xf} + h_{t-1} \cdot W_{hf} + b_f)$ $\Gamma_{o_t} = \sigma(x_t \cdot W_{xo} + h_{t-1} \cdot W_{ho} + b_o)$ $c_t = \Gamma_{f_t} \otimes c_{t-1} + \tilde{c}_t$ $h_t = \Gamma_{o_t} \otimes \tanh(c_t)$
LSTM-NFG		$\tilde{c}_t = \tanh(x_t \cdot W_{x\tilde{c}} + h_{t-1} \cdot W_{h\tilde{c}} + b_{\tilde{c}})$ $\Gamma_{i_t} = \sigma(x_t \cdot W_{xi} + h_{t-1} \cdot W_{hi} + b_i)$ $\Gamma_{o_t} = \sigma(x_t \cdot W_{xo} + h_{t-1} \cdot W_{ho} + b_o)$ $c_t = c_{t-1} + \Gamma_{i_t} \otimes \tilde{c}_t$ $h_t = \Gamma_{o_t} \otimes \tanh(c_t)$

Table A.24: – Continued from previous page

Cell name	Cell architecture	Cell computations
LSTM-NOG		$\tilde{c}_t = \tanh(x_t.W_{x\tilde{c}} + h_{t-1}.W_{h\tilde{c}} + b_{\tilde{c}})$ $\Gamma_{i_t} = \sigma(x_t.W_{xi} + h_{t-1}.W_{hi} + b_i)$ $\Gamma_{f_t} = \sigma(x_t.W_{xf} + h_{t-1}.W_{hf} + b_f)$ $c_t = \Gamma_{f_t} \otimes c_{t-1} + \Gamma_{i_t} \otimes \tilde{c}_t$ $h_t = \tanh(c_t)$
LSTM-NIAF		$\tilde{c}_t = \tanh(x_t.W_{x\tilde{c}} + h_{t-1}.W_{h\tilde{c}} + b_{\tilde{c}})$ $\Gamma_{i_t} = x_t.W_{xi} + h_{t-1}.W_{hi} + b_i$ $\Gamma_{f_t} = \sigma(x_t.W_{xf} + h_{t-1}.W_{hf} + b_f)$ $\Gamma_{o_t} = \sigma(x_t.W_{xo} + h_{t-1}.W_{ho} + b_o)$ $c_t = \Gamma_{f_t} \otimes c_{t-1} + \Gamma_{i_t} \otimes \tilde{c}_t$ $h_t = \Gamma_{o_t} \otimes \tanh(c_t)$
LSTM-NFAF		$\tilde{c}_t = \tanh(x_t.W_{x\tilde{c}} + h_{t-1}.W_{h\tilde{c}} + b_{\tilde{c}})$ $\Gamma_{i_t} = \sigma(x_t.W_{xi} + h_{t-1}.W_{hi} + b_i)$ $\Gamma_{f_t} = x_t.W_{xf} + h_{t-1}.W_{hf} + b_f$ $\Gamma_{o_t} = \sigma(x_t.W_{xo} + h_{t-1}.W_{ho} + b_o)$ $c_t = \Gamma_{f_t} \otimes c_{t-1} + \Gamma_{i_t} \otimes \tilde{c}_t$ $h_t = \Gamma_{o_t} \otimes \tanh(c_t)$
LSTM-NOAF		$\tilde{c}_t = \tanh(x_t.W_{x\tilde{c}} + h_{t-1}.W_{h\tilde{c}} + b_{\tilde{c}})$ $\Gamma_{i_t} = \sigma(x_t.W_{xi} + h_{t-1}.W_{hi} + b_i)$ $\Gamma_{f_t} = \sigma(x_t.W_{xf} + h_{t-1}.W_{hf} + b_f)$ $\Gamma_{o_t} = x_t.W_{xo} + h_{t-1}.W_{ho} + b_o$ $c_t = \Gamma_{f_t} \otimes c_{t-1} + \Gamma_{i_t} \otimes \tilde{c}_t$ $h_t = \Gamma_{o_t} \otimes \tanh(c_t)$
LSTM-NCAF		$\tilde{c}_t = x_t.W_{x\tilde{c}} + h_{t-1}.W_{h\tilde{c}} + b_{\tilde{c}}$ $\Gamma_{i_t} = \sigma(x_t.W_{xi} + h_{t-1}.W_{hi} + b_i)$ $\Gamma_{f_t} = \sigma(x_t.W_{xf} + h_{t-1}.W_{hf} + b_f)$ $\Gamma_{o_t} = \sigma(x_t.W_{xo} + h_{t-1}.W_{ho} + b_o)$ $c_t = \Gamma_{f_t} \otimes c_{t-1} + \Gamma_{i_t} \otimes \tilde{c}_t$ $h_t = \Gamma_{o_t} \otimes \tanh(c_t)$

Table A.24: – Continued from previous page

Cell name	Cell architecture	Cell computations
LSTM-FB1		$\tilde{c}_t = \tanh(x_t \cdot W_{x\tilde{c}} + h_{t-1} \cdot W_{h\tilde{c}} + b_{\tilde{c}})$ $\Gamma_{i_t} = \sigma(x_t \cdot W_{xi} + h_{t-1} \cdot W_{hi} + b_i)$ $b_f = 1$ $\Gamma_{f_t} = \sigma(x_t \cdot W_{xf} + h_{t-1} \cdot W_{hf} + b_f)$ $\Gamma_{o_t} = \sigma(x_t \cdot W_{xo} + h_{t-1} \cdot W_{ho} + b_o)$ $c_t = \Gamma_{f_t} \otimes c_{t-1} + \Gamma_{i_t} \otimes \tilde{c}_t$ $h_t = \Gamma_{o_t} \otimes \tanh(c_t)$
LSTM-CIFG		$\tilde{c}_t = \tanh(x_t \cdot W_{x\tilde{c}} + h_{t-1} \cdot W_{h\tilde{c}} + b_{\tilde{c}})$ $\Gamma_{i_t} = \sigma(x_t \cdot W_{xi} + h_{t-1} \cdot W_{hi} + b_i)$ $\Gamma_{o_t} = \sigma(x_t \cdot W_{xo} + h_{t-1} \cdot W_{ho} + b_o)$ $c_t = (1 - \Gamma_{i_t}) \otimes c_{t-1} + \Gamma_{i_t} \otimes \tilde{c}_t$ $h_t = \Gamma_{o_t} \otimes \tanh(c_t)$
LSTM-PC		$\tilde{c}_t = \tanh(x_t \cdot W_{x\tilde{c}} + h_{t-1} \cdot W_{h\tilde{c}} + b_{\tilde{c}})$ $\Gamma_{i_t} = \sigma(x_t \cdot W_{xi} + h_{t-1} \cdot W_{hi} + c_{t-1} \cdot W_{ci} + b_i)$ $\Gamma_{f_t} = \sigma(x_t \cdot W_{xf} + h_{t-1} \cdot W_{hf} + c_{t-1} \cdot W_{cf} + b_f)$ $\Gamma_{o_t} = \sigma(x_t \cdot W_{xo} + h_{t-1} \cdot W_{ho} + c_t \cdot W_{co} + b_o)$ $c_t = \Gamma_{f_t} \otimes c_{t-1} + \Gamma_{i_t} \otimes \tilde{c}_t$ $h_t = \Gamma_{o_t} \otimes \tanh(c_t)$
LSTM-FGR		$\tilde{c}_t = \tanh(x_t \cdot W_{x\tilde{c}} + h_{t-1} \cdot W_{h\tilde{c}} + b_{\tilde{c}})$ $\Gamma_{i_t} = \sigma(x_t \cdot W_{xi} + h_{t-1} \cdot W_{hi} + \Gamma_{i_{(t-1)}} \cdot W_{ii} + \Gamma_{f_{(t-1)}} \cdot W_{fi} + \Gamma_{o_{(t-1)}} \cdot W_{oi} + b_i)$ $\Gamma_{f_t} = \sigma(x_t \cdot W_{xf} + h_{t-1} \cdot W_{hf} + \Gamma_{i_{(t-1)}} \cdot W_{if} + \Gamma_{f_{(t-1)}} \cdot W_{ff} + \Gamma_{o_{(t-1)}} \cdot W_{of} + b_f)$ $\Gamma_{o_t} = \sigma(x_t \cdot W_{xo} + h_{t-1} \cdot W_{ho} + \Gamma_{i_{(t-1)}} \cdot W_{io} + \Gamma_{f_{(t-1)}} \cdot W_{fo} + \Gamma_{o_{(t-1)}} \cdot W_{oo} + b_o)$ $c_t = \Gamma_{f_t} \otimes c_{t-1} + \Gamma_{i_t} \otimes \tilde{c}_t$ $h_t = \Gamma_{o_t} \otimes \tanh(c_t)$

Table A.25: Description of different architectures of RNN cells.

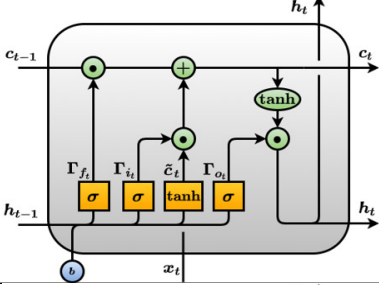
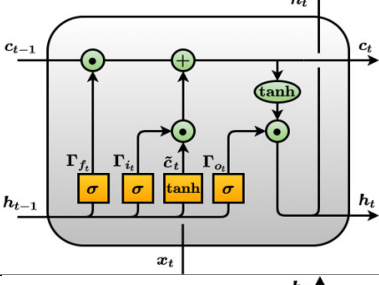
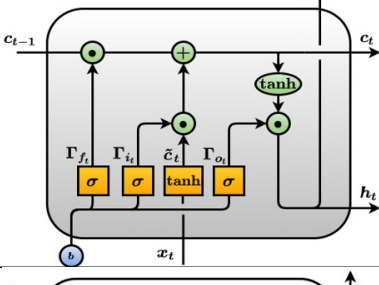
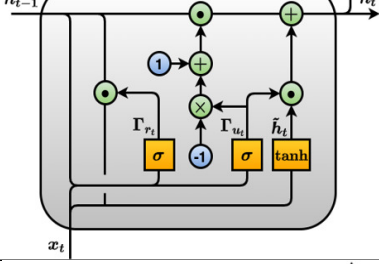
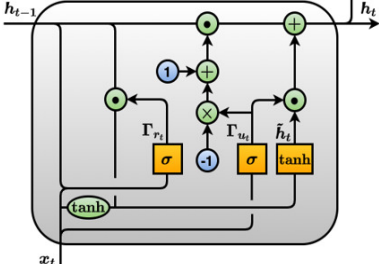
Cell name	Cell architecture	Cell computations
LSTM-SLIM1		$\tilde{c}_t = \tanh(x_t \cdot W_{x\tilde{c}} + h_{t-1} \cdot W_{h\tilde{c}} + b_{\tilde{c}})$ $\Gamma_{i_t} = \sigma(h_{t-1} \cdot W_{hi} + b_i)$ $\Gamma_{f_t} = \sigma(h_{t-1} \cdot W_{hf} + b_f)$ $\Gamma_{o_t} = \sigma(h_{t-1} \cdot W_{ho} + b_o)$ $c_t = \Gamma_{f_t} \otimes c_{t-1} + \Gamma_{i_t} \otimes \tilde{c}_t$ $h_t = \Gamma_{o_t} \otimes \tanh(c_t)$
LSTM-SLIM2		$\tilde{c}_t = \tanh(x_t \cdot W_{x\tilde{c}} + h_{t-1} \cdot W_{h\tilde{c}} + b_{\tilde{c}})$ $\Gamma_{i_t} = \sigma(h_{t-1} \cdot W_{hi})$ $\Gamma_{f_t} = \sigma(h_{t-1} \cdot W_{hf})$ $\Gamma_{o_t} = \sigma(h_{t-1} \cdot W_{ho})$ $c_t = \Gamma_{f_t} \otimes c_{t-1} + \Gamma_{i_t} \otimes \tilde{c}_t$ $h_t = \Gamma_{o_t} \otimes \tanh(c_t)$
LSTM-SLIM3		$\tilde{c}_t = \tanh(x_t \cdot W_{x\tilde{c}} + h_{t-1} \cdot W_{h\tilde{c}} + b_{\tilde{c}})$ $\Gamma_{i_t} = \sigma(b_i)$ $\Gamma_{f_t} = \sigma(b_f)$ $\Gamma_{o_t} = \sigma(b_o)$ $c_t = \Gamma_{f_t} \otimes c_{t-1} + \Gamma_{i_t} \otimes \tilde{c}_t$ $h_t = \Gamma_{o_t} \otimes \tanh(c_t)$
GRU		$\Gamma_{u_t} = \sigma(x_t \cdot W_{xu} + h_{t-1} \cdot W_{hu} + b_u)$ $\Gamma_{r_t} = \sigma(x_t \cdot W_{xr} + h_{t-1} \cdot W_{hr} + b_r)$ $\tilde{h}_t = \tanh(x_t \cdot W_{x\tilde{h}} + (\Gamma_{r_t} \otimes h_{t-1}) \cdot W_{h\tilde{h}} + b_{\tilde{h}})$ $h_t = \Gamma_{u_t} \otimes \tilde{h}_t + (1 - \Gamma_{u_t}) \otimes h_{t-1}$
MUT1		$\Gamma_{u_t} = \sigma(x_t \cdot W_{xu} + b_u)$ $\Gamma_{r_t} = \sigma(x_t \cdot W_{xr} + h_{t-1} \cdot W_{hr} + b_r)$ $\tilde{h}_t = \tanh(\tanh(x_t) + (\Gamma_{r_t} \otimes h_{t-1}) \cdot W_{h\tilde{h}} + b_{\tilde{h}})$ $h_t = \Gamma_{u_t} \otimes \tilde{h}_t + (1 - \Gamma_{u_t}) \otimes h_{t-1}$

Table A.25: – Continued from previous page

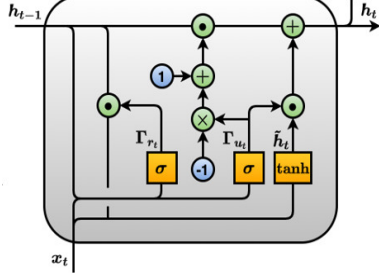
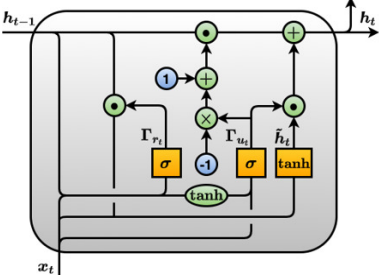
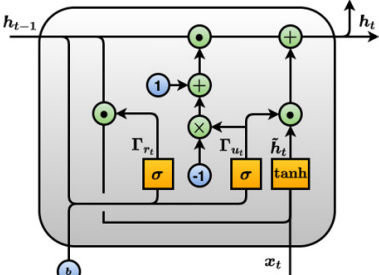
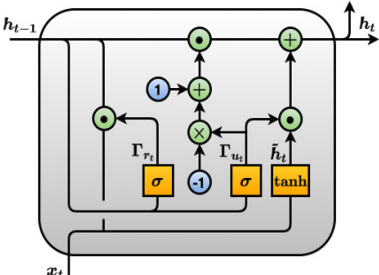
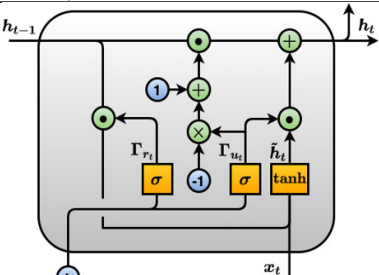
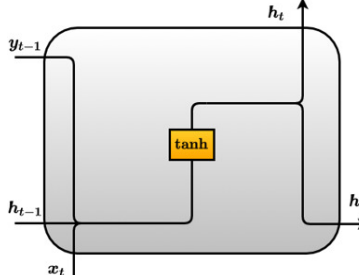
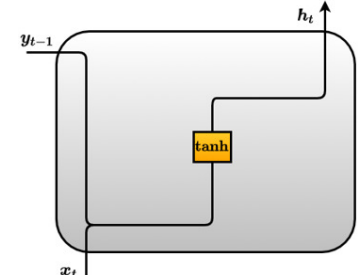
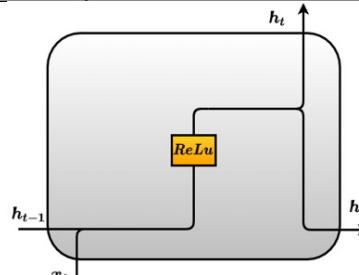
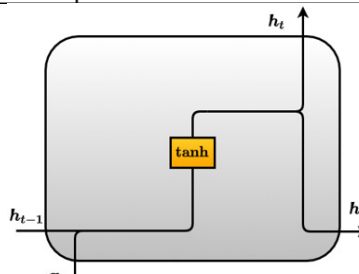
Cell name	Cell architecture	Cell computations
MUT2		$\Gamma_{u_t} = \sigma(x_t \cdot W_{xu} + h_{t-1} \cdot W_{hu} + b_u)$ $\Gamma_{r_t} = \sigma(x_t + h_{t-1} \cdot W_{hr} + b_r)$ $\tilde{h}_t = \tanh(x_t \cdot W_{x\tilde{h}} + (\Gamma_{r_t} \otimes h_{t-1}) \cdot W_{h\tilde{h}} + b_{\tilde{h}})$ $h_t = \Gamma_{u_t} \otimes \tilde{h}_t + (1 - \Gamma_{u_t}) \otimes h_{t-1}$
MUT3		$\Gamma_{u_t} = \sigma(x_t \cdot W_{xu} + \tanh(h_{t-1}) \cdot W_{hu} + b_u)$ $\Gamma_{r_t} = \sigma(x_t \cdot W_{xr} + h_{t-1} \cdot W_{hr} + b_r)$ $\tilde{h}_t = \tanh(x_t \cdot W_{x\tilde{h}} + (\Gamma_{r_t} \otimes h_{t-1}) \cdot W_{h\tilde{h}} + b_{\tilde{h}})$ $h_t = \Gamma_{u_t} \otimes \tilde{h}_t + (1 - \Gamma_{u_t}) \otimes h_{t-1}$
GRU-SLIM1		$\Gamma_{u_t} = \sigma(h_{t-1} \cdot W_{hu} + b_u)$ $\Gamma_{r_t} = \sigma(h_{t-1} \cdot W_{hr} + b_r)$ $\tilde{h}_t = \tanh(x_t \cdot W_{x\tilde{h}} + (\Gamma_{r_t} \otimes h_{t-1}) \cdot W_{h\tilde{h}} + b_{\tilde{h}})$ $h_t = \Gamma_{u_t} \otimes \tilde{h}_t + (1 - \Gamma_{u_t}) \otimes h_{t-1}$
GRU-SLIM2		$\Gamma_{u_t} = \sigma(h_{t-1} \cdot W_{hu})$ $\Gamma_{r_t} = \sigma(h_{t-1} \cdot W_{hr})$ $\tilde{h}_t = \tanh(x_t \cdot W_{x\tilde{h}} + (\Gamma_{r_t} \otimes h_{t-1}) \cdot W_{h\tilde{h}} + b_{\tilde{h}})$ $h_t = \Gamma_{u_t} \otimes \tilde{h}_t + (1 - \Gamma_{u_t}) \otimes h_{t-1}$
GRU-SLIM3		$\Gamma_{u_t} = \sigma(b_u)$ $\Gamma_{r_t} = \sigma(b_r)$ $\tilde{h}_t = \tanh(x_t \cdot W_{x\tilde{h}} + (\Gamma_{r_t} \otimes h_{t-1}) \cdot W_{h\tilde{h}} + b_{\tilde{h}})$ $h_t = \Gamma_{u_t} \otimes \tilde{h}_t + (1 - \Gamma_{u_t}) \otimes h_{t-1}$

Table A.25: – *Continued from previous page*

Cell name	Cell architecture	Cell computations
MGU		$\Gamma_{f_t} = \sigma(x_t \cdot W_{xf} + h_{t-1} \cdot W_{hf} + b_f)$ $\tilde{h}_t = \tanh(x_t \cdot W_{xh} + (\Gamma_{f_t} \otimes h_{t-1}) \cdot W_{hh} + b_{\tilde{h}})$ $h_t = \Gamma_{f_t} \otimes \tilde{h}_t + (1 - \Gamma_{f_t}) \otimes h_{t-1}$
MGU-SLIM1		$\Gamma_{f_t} = \sigma(h_{t-1} \cdot W_{hf} + b_f)$ $\tilde{h}_t = \tanh(x_t \cdot W_{xh} + (\Gamma_{f_t} \otimes h_{t-1}) \cdot W_{hh} + b_{\tilde{h}})$ $h_t = \Gamma_{f_t} \otimes \tilde{h}_t + (1 - \Gamma_{f_t}) \otimes h_{t-1}$
MGU-SLIM2		$\Gamma_{f_t} = \sigma(h_{t-1} \cdot W_{hf})$ $\tilde{h}_t = \tanh(x_t \cdot W_{xh} + (\Gamma_{f_t} \otimes h_{t-1}) \cdot W_{hh} + b_{\tilde{h}})$ $h_t = \Gamma_{f_t} \otimes \tilde{h}_t + (1 - \Gamma_{f_t}) \otimes h_{t-1}$
MGU-SLIM3		$\Gamma_{f_t} = \sigma(b_f)$ $\tilde{h}_t = \tanh(x_t \cdot W_{xh} + (\Gamma_{f_t} \otimes h_{t-1}) \cdot W_{hh} + b_{\tilde{h}})$ $h_t = \Gamma_{f_t} \otimes \tilde{h}_t + (1 - \Gamma_{f_t}) \otimes h_{t-1}$
SCRN		$s_t = (1 - \alpha)x_t \cdot W_{xs} + \alpha \cdot s_{t-1}$ $\alpha \in [0, 1]$ $h_t = \tanh(x_t \cdot W_{xh} + h_{t-1} \cdot W_{hh} + s_{t-1} \cdot W_{sh} + b_h)$

Table A.25: – *Continued from previous page*

Cell name	Cell architecture	Cell computations
MRNN		$h_t = \tanh(x_t \cdot W_{xh} + h_{t-1} \cdot W_{hh} + \hat{y}_{t-1} \cdot W_{yh} + b_h)$
JORDAN		$h_t = \tanh(x_t \cdot W_{xh} + \hat{y}_{t-1} \cdot W_{yh} + b_h)$
IRNN		$h_t = \text{ReLu}(x_t \cdot W_{xh} + h_{t-1} \cdot W_{hh} + b_h)$
ELMAN		$h_t = \tanh(x_t \cdot W_{xh} + h_{t-1} \cdot W_{hh} + b_h)$